A model of productivity for olive orchards

Alejandro Morales Sierra

MSc Thesis Plant Production Systems

PPS-804 24

June 2012

Title:

A model of productivity for olive orchards

Author:

Alejandro Morales Sierra

Thesis:

MSc Thesis Plant Production Systems

PPS-80424

Date:

June 2012

Supervisors:

Peter Leffelaar, Plant Production Systems, Wageningen University (The Netherlands)

Francisco Villalobos, Agronomy Department, University of Cordoba (Spain)

Examiners:

Ken Giller, Plant Production Systems, Wageningen University (The Netherlands)

Table of contents

1. Introduction 1
2. Materials and Methods 2
   2.1. Model 2
      2.1.1. Phenology 4
      2.1.2. Photosynthesis 5
      2.1.3. Respiration 6
      2.1.4. Partitioning of assimilates 7
      2.1.5. Canopy structure 7
   2.2. Calibration 8
      2.2.1. Phenology 9
      2.2.2. Senescence 9
      2.2.3. Canopy photosynthesis 9
      2.2.4. Maintenance respiration 10
      2.2.5. Growth respiration 11
      2.2.6. Partitioning of assimilates 12
      2.2.7. Canopy structure 13
   2.3. Simulations 13
      2.3.1. Case studies 13
      2.3.2. Analysis of simulations 14
3. Results 15
   3.1. Comparison with experiments 15
   3.2. Effect of climate change on high and super-high density olive orchards 19
4. Discussion 22
   4.1. Case 1 22
   4.2. Case 2 23
      4.2.1. Effect of management 24
      4.2.2. Effect of climate 25
5. Recommendations for further research 25
6. Conclusions 26
References 27
Appendix I: Disaggregation of weather data 33
   I.1. Solar radiation 33
      I.1.1. Solar radiation algorithm 33
      I.1.2. Test of the solar radiation algorithm 38
   I.2. Air temperature 38
      I.2.1. Daytime air temperature 38
      I.2.2. Night-time air temperature 40
      I.2.3. Calibration 40

I.3. Vapour pressure deficit 41

Figures

Figure 1: Conceptual diagram describing the model of carbon balance.. 3
Figure 2: A. Simulated and measured leaf area index. 16
Figure 3: A. Simulated and measured fruit production. 16
Figure 4: A. Components of the carbon balance and ratio between respiration and photosynthesis 18
Figure 5: A. Components of the annual carbon balance of the olive trees and adiation use efficiency for total biomass production. 18
Figure 6: Leaf area index under past and future climate. 20
Figure 7: Fruit production under past and future climate. 20
Figure 8: Components of the annual carbon balance of the olive trees 21
Figure 9: A. Ratio between respiration and photosynthesis and radiation use efficiency of total biomass production. 22
Figure A1: Fraction of diffuse after the circumsolar correction. 36
Figure A2: Daytime average solar elevation 37
Figure A3: Fraction of diffuse PAR relative to the uncorrected fraction of diffuse solar radiation. 37
Figure A4: Comparison between simulated and measured solar radiation 38
Figure A5: Air temperature as a function of the parameter I_K. 40
Figure A6: Comparison of measured and simulated values of air temperature. 41
Figure A7: Simulated and measured vapor pressure deficit. 42

Tables

Table 1: Phenological phases for cultivar Arbequina in Cordoba (Spain) 9
Table 2: Parameters of the model of radiation absorption and photosynthesis 10
Table 3: Mass-specific maintenance respiration coefficients. 11
Table 4: Production values and respiration factors 12
Table 5: Partitioning coefficients of assimilates. 12
Table A1: Optimal parameters for the model of air temperature. 41

Abstract

A model of productivity for olive orchards is presented, based on a three-dimensional model of canopy radiation absorption and photosynthesis and the allocation of assimilates to growth and respiration. Assimilates are distributed using partitioning coefficients that vary throughout the year. The effect of pruning on canopy structure is included. The model was tested with measurements of leaf area, biomass production and photosynthesis during the first 4 years of a high density olive orchard cv. 'Arbequina' in Cordoba, Spain. The model overestimated fruit production by 10%, leaf area production by 12% and annual biomass aboveground production by 19%. Four additional simulations were performed to study the effects of management system (high and super-high density olive orchards) and climate (recent climate and future climate projection using the model HadRM3 for scenario A2) on photosynthesis, respiration, biomass production, canopy structure and radiation use efficiency. Under future climate conditions, the increase of photosynthesis was higher than the increase of maintenance respiration, resulting into an increase of radiation use efficiency (on average, 12%) and biomass production (32 and 18% for high and super-high density orchards, respectively). The super-high density orchard always had a higher biomass production than the high density orchard (28 and 13% for recent and future climate projection) but only increased fruit production by 4% under recent climate and decreased fruit production by 8% under future climate projection.

Keywords: *Olea europaea*, superintensive olive, intensive olive, super-high density olive, radiation use efficiency, photosynthesis, respiration.

1. Introduction

Olive trees (*Olea europaea* L.) represent an extended horticultural crop in regions with Mediterranean climate, reaching 9.5 Mha worldwide in 2010 (FAO Statistics Division, 2012). The impact of this crop on the agricultural production of some regions is important, especially in countries where the cultivation of olive trees is done in extensive surfaces such as Spain, Italy or Greece (the production of olives by these countries is 63% of world's production, FAO Statistics Division, 2012). Olive cropping systems, which include agroforestry systems, traditional groves and intensive orchards, at high and super-high densities, are of high relevance from the economic and ecological perspective. The carbon balance of olive trees is responsible for determining the production of oil and biomass. Given that an orchard is a complex system in which the carbon is stored in many different forms, the quantitative study of the system via modelling is a crucial step in understanding its behaviour.

Earlier studies have proposed simple models for the carbon balance of olive trees. Villalobos et al. (2006) proposed to calculate the production of biomass, based on the concept of annual radiation use efficiency and partitioning coefficients, yet this approach does not give insights about the cycling of carbon in the system, its dynamics during the year or the effect of management. Abdel-Razik (1989) proposed a model of potential growth of olive trees based on the growth rate of each type of organ, but did not consider the effects of planting density, canopy structure, pruning or plant age.

Other studies have focused on specific aspects of the carbon cycle, though the results were never integrated in a comprehensive model. Diaz-Espejo et al. (2002) simulated photosynthesis and transpiration of isolated trees using the model RATP (Sinoquet et al., 2001) which scales the fluxes from the leaf to canopy level, but did not consider the mutual shading of neighbouring trees. Diaz-Espejo et al. (2006) calibrated a mechanistic model of photosynthesis, but it did not scale up to the canopy level. Several studies of photosynthesis, transpiration and water use efficiency at the leaf level have been published (for a review, see Connor & Fereres, 2005), as well as agronomic trials comparing yield and vegetative growth for different cultivars, irrigation and planting densities (e.g. De la Rosa et al., 2007; Gomez-del-Campo et al., 2009; Hermoso et al., 2008), but this empirical information has not been integrated into a model of the system.

The objective of this study is to integrate existing quantitative knowledge on the carbon balance of olive threes into a process-oriented model, in order to gain insight on the effect of management and

climate on the productivity of olive orchards as well as identify knowledge gaps that require further research. The model assumes absence of water and nutrient stress and that pests and diseases are not significant. The model is primarily oriented towards intensive olive orchards at high (250-850 trees ha^{-1}) and super-high (1500-3000 trees ha^{-1}) planting densities (Vossen, 2007).

2. Materials and Methods

2.1. Model

The diversity of organs in an olive tree can be classified into six types: leaves, fine branches (i.e. all shoots less than three years old), structural branches (i.e. shoots more than three years old, including the stem), fine roots (i.e. active roots without secondary growth), structural roots (i.e. roots with secondary growth) and fruits (figure 1). This classification was based on the different biochemical composition of the organs, their senescence rate and the effect of phenology on carbon allocation. A three-dimensional model of canopy photosynthesis and radiation absorption generates the daily pool of assimilates that is used for production of new biomass and respiration, which is segregated into maintenance and growth respiration (Cannell & Thornley, 2000). Maintenance respiration is calculated as a function of biomass and temperature and is subtracted directly from the pool of assimilates. The remaining assimilates are distributed among the different organs, based on partitioning coefficients. The loss of carbon during the synthesis of new biomass is included by calculating a production value (Penning de Vries, 1974) for each type of organ, which depends on the biochemical composition of the organ. Senescence of leaves and fine roots is also included, as well as pruning and harvest. A constant specific leaf area is used to convert leaf biomass into leaf area. The different processes are described in detail in Sections 2.1.1 through 2.1.5. The calibration of the model is described in section 2.2.

A state variable is defined for each type of organ, representing the amount of carbon stored per unit of ground surface (g C m^{-2} ground). Since many parameters are defined per unit of dry matter, a carbon concentration (g C g^{-1} DM) is used to switch between carbon and dry matter content. The model operates at two timescales, depending on the flux being simulated (see figure 1, "Continuous Processes" and "Discrete Processes"). Photosynthesis and maintenance respiration are simulated as instantaneous processes by a continuous dynamical modelling approach ("Continuous Processes" in figure 1). The growth of the trees through partitioning of assimilates and the associated growth respiration, as well as senescence, is calculated for every day of the simulation using a discrete dynamical modelling approach ("Discrete Processes" in figure 1). Harvest is a time event (i.e. it is activated the day of harvest for each year of simulation) and pruning is a time and state event (i.e. it is applied the same day as harvest but only if the state variables meet a series of requirements). The events are applied to the discrete part of the model (figure 1).

A discrete dynamical model is a model in which the state variables are updated by applying iteratively a series of rules. When the rules are expressed in the form of equations, they are known as "difference equations". Each iteration corresponds to a time unit that is determined by the definition of the discrete process and not by numerical accuracy. A time unit of one day was chosen for the discrete processes assuming that all the assimilates were consumed within the same day they were produced. A continuous dynamic model is a model in which the state variables are updated by differential equations that are integrated over time. If the analytical solution to the integration is unknown, it has to be approximated numerically. The choice of time step is determined by the trade-off between numerical accuracy (i.e. whether the integration converged or not) and computational time. In this study, a fixed time step (i.e. Euler method) of 30 minutes was chosen for the continuous processes, as smaller time steps had a minimal effect on the integration.

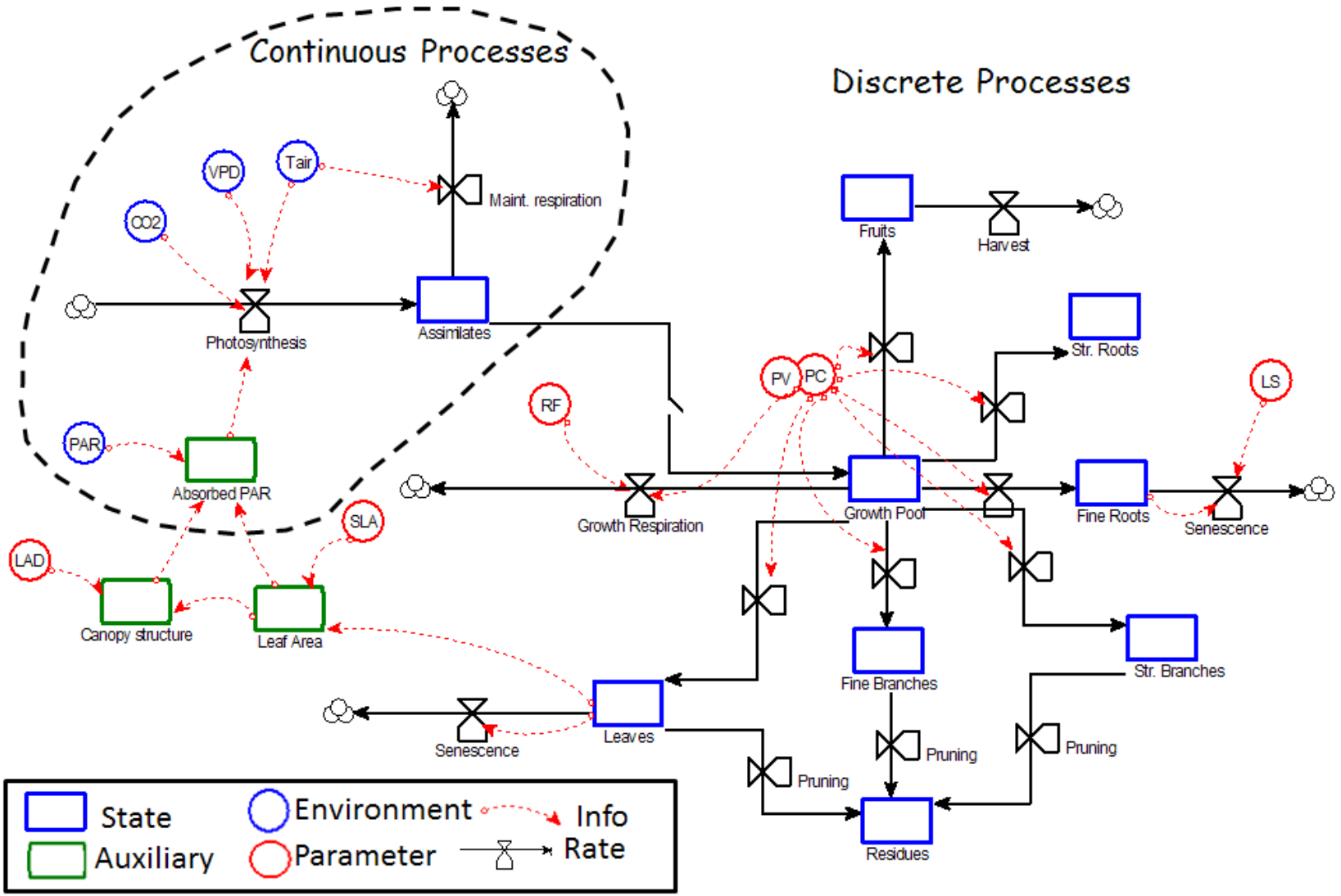

Figure 1: Conceptual diagram describing the model of carbon balance. The diagram is a conceptual scheme and has been simplified to avoid cluttering so it does not include all the variables used within the model. Blue boxes are the state variables that represent the different organs in which carbon is stored. Green boxes are the auxiliary variables associated to canopy structure. Red circles represent parameters and blue circles represent the external variables of the model. The switch symbol represents the transfer of assimilates from the continuous to the discrete sections of the model at the end of each day of simulation. Each arrow represents a flow of carbon into or out of an organ. Assimilates refer to the daily production of photosynthates, whereas growth pool refers to the daily amount of assimilates available for growth. See the text for a detailed description of each variable and parameter. The diagram was built using the software GRIND (van Nes, 2011).

2.1.1. Phenology

2.1.1.1. Phenological phases

The flowering date of olive trees can be calculated with a two-stage phenological model with a first phase when chilling hours (i.e. number of hours when air temperature is below 7 °C) are accumulated and a second phase when thermal time is accumulated (e.g. de Melo-Abreu et al., 2004; Orlandi et al., 2006). However, Ayerza and Sibbett (2001) reported flowering of olive trees without any accumulation of chilling hours near the coast of Peru. Malik and Bradford (2005) also observed flowering without accumulation of chilling hours in chamber studies where air temperature was artificially manipulated. For a given cultivar and location, the range of dates in which flowering occurs is narrow (de Melo-Abreu et al., 2004). Thus, given the contradictory evidence on the effect of temperature on flowering of olive trees, it was preferred to fix flowering date as a parameter of the model rather than simulating it from temperature sum. No quantitative data was found in the literature to calculate the thermal requirements for the other phenological phases (see below). Therefore, the model assumes fixed dates that should be input by the user based on experience with each cultivar and location.

During winter, the aboveground organs of the olive trees do not grow, although, being the olive tree an evergreen plant, photosynthesis still occurs during this period (Testi et al., 2008). Root growth during this period has been reported (Palese et al., 2000; Scariano et al., 2008), but quantitative data are lacking, so its importance cannot be evaluated. Bustan et al. (2011) observed for cv. 'Barnea' in Israel that reserve levels increased in leaves, branches and bark from December until March and decreased during the first months of the growing season, which suggests that they were being used for growth.

Priestley (1977) studied on a monthly basis the biomass and reserve content of leaves, stems and roots of young olive trees and reported that the growth rates of the different organs varied in parallel throughout the year and that reserves were maximum before spring growth, decreasing afterwards, especially in the leaves. Mariscal et al. (2000b) and Scariano et al. (2008) calculated the partitioning coefficients to the different vegetative organs of young olive trees, and did not detect any seasonal variation in the relative allocation to different organs. Villalobos et al. (2006) obtained the partitioning coefficients for young and adult (i.e. fruit-bearing) olive trees at the annual level, reporting no significant change for four consecutive years.

Tombesi (1994) observed that, in the absence of water stress, the daily growth rate of the fruits was constant in the early stages and decreased in the later stages. Moriana et al. (2003) reported that oil content in the fruit was very low (ca. 2%) before day 220 of the year and increased up to 15-20% (on a fresh weight basis) by day 330 of the year. Thus, the reduction of growth rates in the later stages could be explained by a decrease in the production value of the tissue as oil concentration increased and a reduction in assimilate production as days shortened.

All these studies indicate that the partitioning coefficients to the different organs of olive trees are very constant (taking into account that fruits are not always present on the tree and the absence of growth during winter) and variations across experiments and cultivars are constrained to a narrow range.

Based on the empirical evidence presented in the above, 4 phenological phases are distinguished in the model. Phase 1 corresponds to the period of the year when no growth is observed (approximately equal to the winter season) but reserves are being accumulated. During phase 2, all the vegetative organs grow using the assimilates generated by photosynthesis as well as the winter reserves. In phase 3 and 4, assimilates are allocated to both fruits and vegetative organs. During phase 3, the fruits grow with an oil content of only 2%. In phase 4, the growth of the olives is assumed to be composed entirely of oil. At the end of phase 4, the fruits are harvested and pruning is applied, if needed.

All the experiments in which partitioning coefficients were calculated, studied young trees and only Villalobos et al. (2006) obtained data for consecutive years. In that experiment, no alternate bearing of fruits (Lavee, 2007) was observed and the annual partitioning coefficient to fruits was very similar in

the different years. In the long term series of yield for the cv. 'Arbequina' reported by Tous et al. (1998), alternate bearing was only apparent after seven yeras of plantation but it did not follow a regular pattern (results not shown). To the knowledge of the author, it is not known which factors or mechanism is responsible for alternate bearing in olive trees and the empirical evidence indicates that this phenomenon is not always observed. Thus, the model assumes that the partitioning coefficient to fruits is the same for all years of the simulation and, therefore, does not take into account the possible biennial variation in fruit production caused by alternate bearing. The fixed dates that were used to determine the starting and ending points of each phenological phases are shown in Section 2.2.1.

2.1.1.2. Senescence

In the model, root senescence is calculated by assuming that the fine roots can be described as a population of individual roots that die at a constant relative rate:

$$W_{fro,n+1} = W_{fro,n}\left(1 - \frac{\Delta t}{LS}\right) \quad (1)$$

Where W_{fro} is the biomass of fine roots (g DM m^{-2} ground), Δt is the iteration time unit (i.e. one day) and LS is the average life span of the fine roots. The depth of the rooting system is not simulated.

The population of leaves in the model is divided into three different generations, depending on their age. The total leaf biomass is always stored in the state variable W_l but this variable is further segregated into $W_{l,0}$, $W_{l,1}$ and $W_{l,2}$ (g DM m^{-2} ground), where $W_{l,0}$ corresponds to leaves generated in the present year of simulation, $W_{l,1}$ corresponds to leaves generated on the previous year and $W_{l,2}$ corresponds to leaves generated two years before. Each year, leaves belonging to the third generation are shed, given a typical leaf life span of two years for olive trees (Bongi et al., 1987; Proietti, 1998). At the beginning of each year, the leaves are transferred from one generation to the next one (i.e. from $W_{l,0}$ to $W_{l,1}$ and from $W_{l,1}$ to $W_{l,2}$). The new generation of leaves will appear in $W_{l,0}$.

In Italy, Proietti (1998) observed that the abscission of leaves was maximal in June. The same was observed in California by Priestley (1977). In Egypt, Abdel-Razik (1989) reported that relative leaf death rates increased during the spring to a maximum at the beginning of June. The self-shading due to growth of new leaves could trigger senescence as the carbon balance of older leaves becomes more negative. Also, the high demand of assimilates by flowers and fruits during the early stages of reproductive growth could trigger the reallocation of carbon and nutrients from old leaves. Milla et al. (2005) observed that leaf senescence in 8 evergreen Mediterranean species occurred mainly at the end of spring and beginning of summer. Similar conclusions can be deduced from the analysis of 15 Mediterranean evergreen species by Castro-Diez and Monserrat-Marti (1998). Thus, in the model, leaf senescence was assumed to occur during the period May-July when all the leaves in the third generation were eliminated at a constant daily rate (S_{leaf}, g DM m^{-2} ground day^{-1}):

$$S_{leaf} = \frac{W_{lt,2}}{DOY_{SL,2} - DOY_{SL,1}} \quad (2)$$

Where $W_{lt,2}$ is the leaf biomass generated two years before (g DM m^{-2} ground) and $DOY_{SL,1}$ and $DOY_{SL,2}$ are the days of the year when leaf senescence begin and end, respectively.

2.1.2. Photosynthesis

Photosynthesis is calculated using the model of canopy photosynthesis and radiation absorption 'Maestra' (Luo et al., 2001). 'Maestra' calculates the absorption of radiation of a three-dimensional canopy assuming that the crowns of the trees can be described by regular shapes (e.g. cones, prisms, cylinders, etc.). For high density olive orchards, the crowns are described by ellipsoids and for super-high density olive orchards, rectangular prisms are used. The model calculates photosynthesis at different points within the crown of a target tree located in the centre of a virtual plot.

The absorption of PAR radiation is computed using the method proposed by Norman and Welles (1983). Photosynthesis is obtained as the result of coupling a model of CO_2 biochemical demand (Farquhar et al., 1980) and stomatal conductance (Leuning, 1995). It is assumed that air temperature and vapour pressure deficit do not vary within the canopy and that the boundary layer resistance of the leaves is negligible (Jarvis and McNaughton, 1986). It is further assumed that the leaf area density and the photosynthetic capacity of the leaves do not vary within the canopy. The distribution of leaf angles is described by an ellipsoid as proposed by Campbell (1986). Support for such assumptions when simulating canopy photosynthesis of olive trees have been discussed in Morales (2012).

The model calculates photosynthesis every 30 minutes, but weather data is generally available only at the daily scale. Thus, the daily weather input is disaggregated into values every 30 minutes. The algorithms of Spitters et al. (1986), Goudriaan & van Laar (1994) and Ephrat et al. (1996) are used. The equations are described in detail in Appendix I, along with a comparison of the disaggregated values with a one-year long weather dataset.

The simulations of photosynthesis and radiation absorption by the model 'Maestra' have been tested for a super-high density olive orchard using the same parameterization as in the present study (Morales, 2012). Mariscal et al. (2000a) built a model of radiation absorption based on the same theory that was tested with a high density olive orchard.

2.1.3. Respiration

The respiration of olive trees can be separated into a component associated to the growth of new biomass (growth respiration) and the maintenance of existing biomass (maintenance respiration). Growth respiration depends on the amount of biomass produced and the biochemical composition of the new biomass (Penning de Vries et al., 1974), whereas maintenance respiration is associated to the active transport of solutes, protein turnover and cellular repair (Cannell & Thornley, 2000) and varies with biomass, nitrogen content and temperature. However, there is not a clear mechanistic division between these two types of respiration and different experimental methods exist for their quantification. See section 2.2.4 and 2.2.5 for details on the calibration of the two respiratory components.

The response of maintenance respiration to temperature is described by the expression:

$$R_{m,k} = W_k R_{ms,k} Q_{10}^{(T_{air}-25)/10} \quad (3)$$

Where $R_{m,k}$ is the maintenance respiration of organ k (g C m^{-2} ground h^{-1}), W_k is the biomass stored in organ k (g DM m^{-2} ground), $R_{ms,k}$ is the respiration coefficient of organ k at 25 °C (g C g^{-1} DM h^{-1}), Q_{10} is the factor by which maintenance respiration is increased for an increase of 10 °C and T_{air} is the temperature of the air (°C). The approach taken in this study assumes that the maintenance respiration of all the structural biomass (i.e. structural roots and branches) can be described by an unique maintenance respiration coefficient. This will approach will tend to overestimate total plant maintenance respiration as the virtual trees accumulate structural biomass.

For every organ and based on its biochemical composition, an organ-level production value (PV_o, g DM g^{-1} C) is calculated. The production value represents the amount of biomass produced per unit of assimilate used for growth (Loomis et al., 2011) and it is calculated as:

$$PV_o = \frac{1}{\sum_{\forall i} f_i \frac{1}{PV_i}} \quad (4)$$

Where f_i is the fraction of component i and PV_i is the production value of component i. The respiration fraction (RF, g C g^{-1} C), which represents the fraction of assimilate carbon that is lost in respiration, is calculated as $RF = CPF_o\ PV_o$ where CPF_o is the CO_2 production factor (g C g^{-1} DM), that quantifies the amount of growth respiration per unit of growth of each organ (Loomis, 2011). The

values of CPF_o were calculated from the biochemical composition of each organ and component-specific published values (Loomis, 2011) in an analogous way to PV_o.

2.1.4. Partitioning of assimilates

The total daily integrated maintenance respiration is obtained from integrating equation 3 over the day and aggregating for all organs:

$$R_{mD} = \sum_{k=1}^{6} \left(W_k R_{ms,k} \int_0^{24} Q_{10}^{(T_{air}(t)-25)/10} dt \right) \quad (5)$$

Where R_{mD} is the daily demand of assimilates for maintenance respiration (g C m^{-2} ground). The actual maintenance respiration (R_m, g C m^{-2} ground) will be the minimum of the potential demand and the assimilates generated by photosynthesis (i.e. $R_m = \min(Pool_a, R_{mD})$). Once maintenance respiration has been covered, the remaining assimilates (i.e. $Pool_g = Pool_a - R_m$) are allocated to the different organs k and transformed into dry matter using the corresponding production value:

$$W_{k,n+1} = W_{k,n} + Pool_g PC_k PV_{o,k} \quad (6)$$

Where PC_k (g C g^{-1} C) is the partitioning coefficient for organ k. The growth respiration associated to each organ k ($R_{g,k}$, g C m^{-2} ground) is calculated as:

$$R_{g,k} = Pool_g PC_k RF_k \quad (7)$$

And the total daily growth respiration is obtained by aggregating for all the organs. Note that neither maintenance nor growth respiration have units of time and the reason is because, in a discrete model, one does not calculate rates of change, but rather the total change after a fixed period of time, in this case, a day (see Section 2.1 for further details).

2.1.5. Canopy structure

The growth of leaf area index is calculated from the growth of leaf biomass using a constant specific leaf area (SLA, m^2 leaf g^{-1} DM):

$$LAI_{n+1} = LAI_n + Pool_g PC_l PV_{o,l} SLA \quad (8)$$

Where LAI is the leaf area index (m^2 leaf m^{-2} ground), PC_l is the partitioning coefficient for leaves (g C g^{-1} C) and PV_l is the production value for leaves (g DM g^{-1} C). In addition to the leaf area index, the leaf area density (i.e. leaf area per unit of canopy volume), the canopy volume and the shape of the crowns are needed to calculate the absorption of radiation by the model 'Maestra'.

The crown of an olive tree in a high density olive orchards can be approximated by an ellipsoid (Mariscal et al., 2000a). The shape of the ellipsoid is determined by the ratio between vertical and horizontal radius. It is assumed that the trees conserve this ratio as they grow. Each day of the simulation, the crown volume is calculated from the leaf area index, leaf area density and planting density. Then, the dimensions of the crowns are determined from the formula of the volume of an ellipsoid.

Villalobos et al. (2006) observed that, during the first 4 years of a high density plantation of olive trees cv. 'Arbequina' that were not pruned, the leaf area density was constant at 2 m^2 leaf m^{-3} crown. No other experiment exists (to the knowledge of the author) where the evolution of leaf area density for non-pruned olive trees is reported.

Pruning strategies in high density olive orchards focus on reducing the leaf area density to facilitate the penetration of light into the canopy. It is assumed that the commonly observed decrease of leaf area density with canopy volume in olive orchards (e.g. Villalobos et al., 1995; Orgaz et al., 2007) is

generated by pruning and does not represent the natural behaviour of the olive tree. Orgaz et al. (2007) proposed an empirical model to describe the relationship between leaf area density and crown volume:

$$LAD_t = \begin{cases} 2 & if\ V_u \le 0.5 \\ 2 - \dfrac{0.8(V_u - 0.5)}{1.5} & if\ V_u > 0.5 \end{cases} \quad (9)$$

Where LAD_t is the leaf area density (m^2 leaf m^{-3} crown) and V_u is the canopy volume per unit of ground of surface (m^3 crown m^{-2} ground). In the model, at the end of phase 4 of each year of simulation, the value of LAD_t is calculated and pruning is applied to reduce the leaf area density of the trees down to this value. The growth of new leaves during the next year is assumed to occur with a leaf area density of 2 m^2 m^{-3} crown, but it is assumed that the new growth is uniformly distributed within the crowns, so that the assumption of an uniform leaf area density would still hold. Thus, during the next year after a pruning is executed, both the canopy volume and the leaf area density will increase due to new leaf area growth.

The maximum height of a high density orchard is also limited to ensure that all operations (e.g. harvesting and spraying) can be performed adequately. Whenever the height of the trees at the end of phase 4 exceeds a user-given maximum value, the trees are pruned down to the maximum height and the volume is reduced in order to maintain the same crown shape as before the pruning (i.e. same ratio between vertical and horizontal radii). This means that, whether pruning is actually applied or not and the amount of biomass removed depends on the leaf area density and height of the trees at the end of phase 4. The model does not include "green pruning" or summer pruning that is sometimes used in olive trees. Also, it assumes that pruning is instantaneous and the application of strict rules to determine the application or not of pruning may cause unrealistic simulations (i.e. in reality, farmers do not have strict rules and pruning strategies may vary for different locations).

It is assumed that the leaf area removed by pruning affects equally all the generations of leaves. Pruning also eliminates part of the biomass stored in structural and fine branches, depending on the pruning intensity. It is assumed that the ratio between the biomass of structural branches and leaves and between fine branches and leaves does not change with pruning. This allows calculating the biomass removed from the different types of organs as a function of pruned leaf area. The response of the root system to pruning (Cannell & Dewar, 1994) was not included in the model, as no reference was found in the literature for olive trees.

In super-high density olive orchards, the crown of each tree can be approximated by a rectangular prism, where the ratio of height and width of the crown also defines the shape. Because the pruning of super-high density orchards is applied mechanically using blades and discs, it is assumed that only the volume and not the leaf area density is modified. As leaf area density does not vary, pruning is applied only when the height exceeds a maximum value, and lateral pruning is used to maintain the ratio between height and width of the hedgerow. The reiteration of this type of mechanical pruning every year prevents the formation of structural branches beyond the maximum height and width, so that only fine branches are removed each time. It was assumed that the different generations of leaves were uniformly distributed throughout the canopy. As in high density orchards, it is assumed that the ratio between fine branches and leaves did not change with pruning.

2.2. Calibration

The calibration of the model was achieved using data from the literature. The phenology and management-related parameters were chosen for a typical intensive olive orchard in Cordoba, Spain (37.8º N, 4.8º W, 110 m above the sea level. Mediterranean climate). All the data used to calibrate the model was gathered in experiments were the trees were irrigated, fertilized and weeds and pests were controlled adequately.

2.2.1. Phenology

The dates describing the starting and ending dates of the different phenological phases of olive trees (Section 2.1.1.1) were determined (table 1) for cv. 'Arbequina' in the area of Cordoba, Spain, based on the observations from different experiments (Moriana et al., 2003; Testi et al., 2008; Villalobos et al., 2006). As indicated previously, the lack of proper scientific information regarding the thermal requirement of the different phenological phases in olive trees justifies the use of location and cultivar-specific fixed dates.

Table 1: Phenological phases proposed for the model of carbon balance, parameterized for cv. 'Arbequina' in Cordoba (Spain).

Phase	Description	Day of Year
1	No growth	331-365 1-45
2	Vegetative growth	46-150
4	1st phase fruit growth	151-220
5	2nd phase fruit growth	221-330

2.2.2. Senescence

No data was found regarding the senescence of fine roots in olive trees. By comparison with other species, the average life span of fine roots (*LS* in equation 1) was assumed constant and equal to 90 days. Fine roots of Mediterranean evergreen oaks (*Quercus ilex* L.) have a median life span of 67 days under natural conditions (Lopez et al., 2001). Eissenstat and Yanai (1997) reported life spans between 90 and 152 days for the fine roots of different species of the genus *Citrus*.

Based on the observations reported in the literature (Abdel-Razik, 1989; Priestley, 1977; Proietti, 1998), the starting and ending date of the period when leaf senescence occurs ($DOY_{SL,1}$ and $DOY_{SL,2}$ in equation 2) were assumed to be the days 120 and 190 of the year.

2.2.3. Canopy photosynthesis

The values for the parameters of the model of canopy photosynthesis and radiation absorption were taken from the study of Morales (2012), where the model was validated against measurements of canopy photosynthesis and radiation absorption in a super-high density olive orchard using cv. 'Arbequina' (table 2). In Morales (2012), the parameters had been taken themselves from the scientific literature (see Source in table 2).

Moriana et al. (2002) calibrated the stomatal conductance model of Leuning (1995) using cv. 'Picual' and Diaz-Espejo et al. (2006) used cv. 'Manzanilla' to calibrate the photosynthesis model of Farquhar et al. (1980). To the knowledge of the author, no model of leaf photosynthesis or stomatal conductance has been published for cv. 'Arbequina', but the differences in leaf photosynthesis among cultivars are considered to be small (Connor & Fereres, 2005).

Table 2: Parameters needed for the simulation of canopy photosynthesis. ρsoil, τleaf and ρleaf are the soil reflectance, leaf transmittance and reflectance of PAR, respectively. gs0 is the stomatal conductance for null net photosynthesis, a1 is the proportionality factor between net photosynthesis and stomatal conductance, D0 describes the response of stomatal conductance to VPD, Γ is the CO2 compensation point, θ describes the degree of curvature of the response to PAR of the electron transport rate, α is the quantum efficiency, Jmax and Vc,max are the maximum rates of electron transport and activity of Rubisco. HJ and HVc are the activation energies of Jmax and Vc,max. Rd and HRd are the reference leaf respiration at 25 °C and its activation energy. The units in this table correspond to the original units in Maestra and may differ from the ones used in the rest of the text.

Parameters	Units	Nominal value	Source
ρ_{soil}	–	0.2	Assumed
τ_{leaf}	–	0.001	Mariscal et al. (2000a)
ρ_{leaf}	–	0.072	Mariscal et al. (2000a)
g_{s0}	mol m^{-2} leaf s^{-1}	0.045	Moriana et al. (2002)
a_1	–	4.53	Moriana et al. (2002)
D_0	Pa	3500	Moriana et al. (2002)
Γ	μmol CO_2 mol^{-1}	46	Moriana et al. (2002)
θ	–	0.9	Diaz-Espejo et al. (2006)
α	mol e (mol PAR)$^{-1}$	0.2	Diaz-Espejo et al. (2006)
J_{max}	μmol m^{-2} leaf s^{-1}	135.5	Diaz-Espejo et al. (2006)
$V_{c,max}$	μmol m^{-2} leafs^{-1}	82.7	Diaz-Espejo et al. (2006)
R_d	μmol m^{-2} leaf s^{-1}	1.12	Diaz-Espejo et al. (2006)
H_J	J mol^{-1}	35 350	Diaz-Espejo et al. (2006)
H_{Vc}	J mol^{-1}	73 680	Diaz-Espejo et al. (2006)
H_{Rd}	J mol^{-1}	44 790	Diaz-Espejo et al. (2006)

2.2.4. Maintenance respiration

Perez-Priego et al. (*submitted*) measured maintenance respiration of olive trees with a closed chamber after keeping the plants in the darkness for 48 hours. The different organs in the trees were removed sequentially and weighted and several measurements at different temperatures were performed in between. The maintenance respiration coefficients at 25 °C for leaves, fine branches, structural branches and fruits were 0.80 10^{-4}, 0.24 10^{-4} , 0.05 10^{-4} and 0.67 10^{-4} g C g^{-1} DM h^{-1}, respectively.

Merino (1987) reported a maintenance respiration coefficient for leaves of 2.16 10^{-4} g C g^{-1} DM h^{-1} at 20 °C. Assuming a Q_{10} of 2 this value is equivalent to 3.20 10^{-4} g C g^{-1} DM h^{-1}, which is four times bigger than the value obtained by Perez-Priego et al. (*submitted*). Abdel-Razik (1989) estimated maintenance respiration coefficients at 25 °C from nitrogen and mineral contents, obtaining 1.25 10^{-4}, 0.87 10^{-4}, 1.12 10^{-4} and 3.50 10^{-4} g C g^{-1} DM h^{-1} for leaves, fine branches, fine roots and fruits, respectively. These values are also larger than the ones obtained by Perez-Priego et al. (*submitted*), especially for the case of fruits. Fruits can reassimilate 40-80% of the respired CO_2 (Proietti et al., 1999) which could explain the much higher maintenance coefficient found by Abdel-Razik (1989) as the reassimilation is implicit in the chamber measurements. Thus, it does not seem adequate to estimate the maintenance respiration of fruits based on nitrogen content, unless the reassimilation is also simulated.

The value reported by Abdel-Razik (1989) for leaf respiration is based on a nitrogen concentration of 1.7%, which is a reasonable value for well-fertilized olive orchards (Fernandez-Escobar et al., 2009). The respiratory processes included in the concept of maintenance respiration are not completely independent from growth (Cannell & Thornley, 2000), so that the rates of respiration published by Perez-Priego et al. (*submitted*) could be underestimated due to the absence of growth. The final choice of parameters (table 3) combined the values reported for leaves, fine branches and fine roots by Abdel-Razik (1989) and for fruits and wood by Perez-Priego et al. (*submitted*). The reason for such

choice is that the maintenance respiration of structural branches and stem was not calculated by Abdel-Razik (1989) and that the coefficients reported by Perez-Priego et al. (*submitted*) for fruits include, implicitly the correction for reassimilation of CO_2. Still, it is important to recognize that there is a high uncertainty about the values to be assigned to these parameters.

Maintenance respiration of structural branches depends on the biomass of the outer layers of xylem (i.e. sapwood), as the maintenance of the inner layers of xylem is negligible (Ryan, 1990). Since the amount of sapwood was not reported, the coefficient was applied to all the biomass contained in structural branches, which causes an underestimation of maintenance respiration in smaller trees compared to the one used in the original experiment (Perez-Priego et al., *submitted*), although this would have a minor impact on the simulation given the very small coefficient associated to structural branches. However, it may generate an important overestimation for large plants in long simulations.

Perez-Priego et al. (*submitted*) used the model of Lloyd and Taylor (1994) which assumes that the sensitivity of respiration to temperature decreases with temperature. With the parameter values reported in the original article, the model was very similar to using a Q_{10} = 2, in the range of temperatures 20 - 35 °C.

Table 3: Mass-specific maintenance respiration coefficients measured with chambers after 48 hours of darkness and parameters of describing temperature response from the model of Lloyd & Taylor (1994). Modified from Perez-Priego et al. (*submitted*) and Abdel-Razik (1989) assuming a Q_{10} = 2.

Organ	**Rm at 25 °C (10^{-4} g C g^{-1} DM h^{-1})**
Leaves	1.25
Fine branches	0.87
Structural branches	0.05
Fruits	0.67
Structural roots	0.05
Fine roots	1.12

2.2.5. Growth respiration

The biochemical composition of leaves, fine and structural branches were taken from Mariscal et al. (2000b), but the fraction of lignin in structural branches was set to 0.2 based on published analyses of the wood of olive trees (Ruiz et al., 2006; Ververis et al., 2004). The composition of the fruit was taken from Zamora et al. (2001). Note that two phases are being distinguished in the growth of fruits (see Section 2.1.1.1) and they have different production values and respiration factors (table 4). Structural and fine roots were assumed to have the same biochemical composition as structural and fine branches, respectively. The reserves of olive trees are mainly located in leaves and stems (Bustan et al., 2011; Priestley, 1977) and they consist primarily of sucrose, mannitol and starch (Bustan et al., 2011; Connor & Fereres, 2005; Priestley, 1977). Thus, the production value and respiration factors were calculated assuming a 100% carbohydrate content (table 4).

The biochemical composition of each organ was corrected by its mineral content (Vertregt and Penning de Vries, 1987). The production values and respiration factors for each biochemical component were taken from Loomis et al. (2011). The different organs had similar production values and respiration factors except for the fruits during the phase of oil accumulation and the winter reserves. The carbon concentration in the organs (CC, g C g^{-1} DM), was calculated as $CC = (1 - RF_o)/PV_o$ and was approximately equal to 0.55 g C g^{-1} DM for the different organs.

Mariscal et al. (2000b) estimated very similar production values to the ones obtained in this study for leaves and fine branches, but slightly smaller for structural branches (1.72 g DM g^{-1} C) due to the assumption of a 30% lignin content. Merino (1987) reported a leaf production value of 1.50 g DM g^{-1} C. Abdel-Razik (1989) reported higher production values for leaves (2.00 g DM g^{-1} C), very similar values for fine branches and roots (1.60 g DM g^{-1} C), and much lower values for structural branches (1.20 g DM g^{-1} C) due to the assumption of a much higher lignin content. Such a high leaf production value seems unlikely as olive trees are sclerophyllous evergreen plants, which tend to have lower

production values than deciduous and herbaceous plants (Merino, 1987), due to their higher lignin content (in this case, 18.4% on dry matter).

Table 4: Production values and respiration factors of the different organs included in the model. The values for fruit correspond to oil contents of 2% (left) and 100% (right).

Organ	PV (g DM (g C)$^{-1}$)	RF (g C (g C)$^{-1}$)
Leaves	1.67	0.300
Fine branches	1.72	0.227
Structural branches	1.80	0.143
Fruits	1.85 – 0.92	0.32 – 0.41
Structural roots	1.80	0.143
Fine roots	1.72	0.227
Reserves	2.07	0.067

2.2.6. Partitioning of assimilates

Information regarding the partitioning of assimilates was obtained from different experiments that studied irrigated trees in pots or in the field. Villalobos et al. (2006) calculated the partitioning coefficients to the different organs aboveground in a high density orchard cv. 'Arbequina', by means of linear regression between cumulative biomass of the different organs. The fraction allocated to leaves, structural branches, fine branches and fruits were 0.16, 0.10, 0.24 and 0.50, respectively. Mariscal et al. (2000b) reported in 1-year old olive trees partitioning coefficients of 0.24, 0.5 and 0.26 for leaves, structural branches and roots. Scariano et al. (2008) reported for 3-year old potted olive trees a partitioning of 0.31 to roots (0.20 to structural roots, 0.11 to fine roots), 0.28 to leaves, 0.14 to fine branches and 0.21 to structural branches. Based on these results, the partitioning coefficients (table 5) for the organs aboveground were taken from Villalobos et al. (2006) and, for organs belowground, from Scariano et al. (2008).

Note that the partitioning coefficient to fruits obtained by Villalobos et al. (2006) was defined at the annual level, though fruits do not grow during the entire year. It was assumed that the partitioning coefficient to fruits during phases 3 and 4 were the same, though they had to be modified by the production values of fruits in each phase. From the starting and ending dates of the phenological phases used in the model (see Section 2.2.1.), it was derived that fruits are growing during 63% of the total growing season. Assuming that the average daily biomass production is 30% lower for the period of fruit growth compared to the entire growing season (this was estimated from simulations, where the decrease is caused primarily by maintenance respiration), the average daily partitioning coefficient should be 0.85 g DM g^{-1} DM, in order to obtain an annual value of 0.5 g DM g^{-1} DM. Once corrected for the production values, it corresponds to 0.85 and 0.95 g C g^{-1} C in phenological phases 3 and 4, respectively. Therefore, the vegetative organs only receive 15 and 5% of the assimilates available for growth during phases 3 and 4, and the partitioning coefficient for each vegetative organ (table 5) are modified by these fractions.

Table 5: Partitioning coefficients of assimilates to the different organs and reserve pool, corrected for production values and for the different phenological phases.

Organ	Partitioning coefficients (g C g^{-1} C)			
	Phase 1	Phase 2	Phase 3	Phase 4
Leaves	0.00	0.22	0.03	0.010
Fine branches	0.00	0.14	0.02	0.007
Structural branches	0.00	0.33	0.05	0.016
Fruits	0.00	0.00	0.85	0.95
Structural roots	0.00	0.20	0.03	0.010
Fine roots	0.00	0.11	0.02	0.007
Reserves	1.00	0.00	0.00	0.000

2.2.7. Canopy structure

For the application of pruning, the model assumed a maximum height of 5 and 2.5 m for high density and super-high density olive orchards, respectively. The natural leaf area density was assumed equal to 2 m^2 leaf m^{-3} crown (Villalobos et al., 2006). It was assumed a ratio between vertical and horizontal radius of 1.1 (Villalobos et al., 2006). By default, a specific leaf area of 5 10^{-3} m^2 leaf g^{-1} DM was assumed (Mariscal et al., 2000b; Morales, 2012). However, in Section 2.3.1.1, where the model is compared to the measurements reported by Villalobos et al. (2006), the measured specific leaf area (4.2 10^{-3} m^2 leaf g^{-1} DM) was used instead.

2.3. Simulations

2.3.1. Case studies

2.3.1.1. Case 1: Comparison with experiment in Villalobos et al. (2006)

As a test, the model was used to predict the growth and development of the experimental high density olive orchard studied by Villalobos et al. (2006). The simulations of biomass and canopy structure were compared to the results obtained in the experiment. The experiment was performed in a 4-ha plot planted with olive trees cv. 'Arbequina' in Cordoba, Spain (37.8º N, 4.8º W, 110 m above the sea level), with a typical Mediterranean climate. The trees were planted at the end of 1997, with a planting density of 408 tree ha^{-1}, with a distance between rows of 7 m and 3.5 m between consecutive trees within each row. The rows were oriented along the North-South axis. Irrigation was localized with drippers (Testi et al., 2008) at the base of each tree.

Leaf area index and canopy volume were measured at regular intervals during the period 1998-2002. The biomass of the different organs aboveground was measured in March 1999, December 1999, December 2000 and December 2001. Each measurement of biomass consisted of a sample of 5 trees that were cut down to the ground level and the dry matter content of fruits, leaves, fine branches and structural branches was measured. Radiation absorption was calculated from measurements of canopy dimensions and a detailed model calibrated for the same orchard (Mariscal et al., 2000a). From the measurements of biomass and radiation absorption, the radiation use efficiency for aboveground biomass production was calculated. The trees in this experiment did not show alternate bearing of fruits.

The model was initiated at the beginning of year 1998, using as initial value the reported leaf area index and estimating the biomass of the different organs from the partitioning coefficients. Because the trees in the experiment were not pruned, the part of the model dedicated to simulating pruning was deactivated. The weather input was taken from the daily weather data gathered by a weather station in the area (less than 1 km away from the experimental plot).

2.3.1.2 Case 2: Effect of climate change and planting density on carbon balance

The model was used to analyse the dynamics of biomass accumulation, radiation use efficiency, respiration and photosynthesis in high density and super-high density olive orchards under recent climate conditions (1960-1975) and projected future climate conditions (2070-2085). The projections were generated by the regional (i.e. grid cell of 50x50 km^2) climate model HadRM3 (Pope et al., 2000), for the emission scenario A2 (IPCC, 2007) in the area of Cordoba, Spain.

The output of HadRM3 consists on daily weather variables that coincide with the input required by the model (i.e. solar radiation, maximum and minimum temperature, average wind speed and vapour pressure). A constant CO_2 concentration of 740 ppm was assumed (i.e. the average for the period 2070-2085 for the scenario A2). The initial values for the state variables were the same as for Case 1, as they represent typical plants for the first year of an olive plantation.

2.3.2. Analysis of simulations

The simulations generated in each case study were analysed in detail, focusing on the dynamics of canopy structure, fruit production, photosynthesis and maintenance and growth respiration. In addition, the radiation use efficiency at the annual scale was calculated from the output (Section 2.3.2.1) as well as the ratio between total respiration and photosynthesis (Section 2.3.2.2) which was compared to the theoretical limits calculated by the equations proposed by van Oijen et al. (2010).

2.3.2.1. Analysis of radiation use efficiency

Villalobos et al. (2006) proposed to calculate the productivity of irrigated olive orchards using the concept of radiation use efficiency, that is, the ratio between biomass production and absorbed PAR (RUE, g DM MJ^{-1} PAR). The concept of radiation use efficiency can be extended to the production of any type of organ (i.e. radiation use efficiency for leaves, fruits, wood, etc.).

From the perspective of carbon sequestration, it is interesting to calculate the radiation use efficiency for the production of total plant biomass (including belowground organs). This is defined as:

$$RUE = \frac{\Delta W_T}{aPAR} \tag{10}$$

Where ΔW_T is the gross increase (i.e. corrected for losses due to pruning, harvest and senescence) of plant biomass (g DM m^{-2} ground) in each year of the simulation and *aPAR* is the total amount of PAR absorbed by the canopy during the year (MJ PAR m^{-2} ground).

From an agronomical perspective, it is interesting to calculate the radiation use efficiency for the production of oil, as this is the main product obtained from an olive orchard. In the model, olive oil is produced during the phenological phase 4, so that the radiation use efficiency can be calculated as:

$$RUE_{oil} = \frac{\sum_{i=DOY_{P,3}}^{DOY_{P,4}} \Delta W_{fr,i}}{aPAR} \tag{11}$$

Where $\Delta W_{fr,i}$ is the increase of fruit biomass on day i of the year (g DM m^{-2} ground), $DOY_{P,3}$ and $DOY_{P,4}$ are the days when the phenological phase 4 starts and ends, respectively. The effect of plant age (for both case studies), management system and climate (only for Case 2) on both radiation use efficiencies were analysed.

2.3.2.2. Analysis of respiration and photosynthesis

Empirical evidences indicate that the ratio between plant respiration and photosynthesis is constrained to a narrow range, especially when averaged for long periods of time (Cannell & Thornley, 2000; van Oijen et al., 2010). For example, Gifford (1995) cultivated wheat plants at constant temperature and CO_2 concentration, and observed that the ratio between daily respiration and photosynthesis did not vary with CO_2 concentration and only increased from 0.40 to 0.43 as temperature doubled. DeLucia et al. (2007) observed that, for different forests, the net primary production (i.e. the difference between photosynthesis and respiration) increased linearly with photosynthesis with a slope of 0.53, using data extracted from 26 published studies. However, when DeLucia et al. (2007) analysed individual cases, there was an increase in the ratio with the age of the forest and the observed ratios varied from 0.17 up to 0.77. This suggests that this ratio may be highly variable in tree systems. In the model presented in this study, photosynthesis and respiration are simulated independently, as functions of environmental variables, which does not ensure that the ratio between respiration and photosynthesis will be constrained within realistic values (Cannell & Thornley, 2000; van Oijen, 2010).

van Oijen et al. (2010) proposed a series of simple mathematical equations to describe the relative magnitudes of photosynthesis, growth respiration and maintenance respiration based on the

conservation of mass in a plant (excluding senescence and root exudation). The analysis is based on the following 5 equations:

$$NPP = P - R_g - R_m \quad (12)$$

$$NPP = G + S \quad (13)$$

$$R_g = G\left(1 - Y_g\right) / Y_g \quad (14)$$

$$\rho = \left(R_g + R_m\right) / P \qquad \text{for } 0 < \rho < \infty \quad (15)$$

$$\alpha = \frac{S}{P} \qquad \text{for } -\infty < \alpha < 1 \quad (16)$$

Where *NPP* is the total daily net primary production (g C m^{-2} ground), *P* is daily canopy photosynthesis (g C m^{-2} ground), R_g is daily growth respiration (g C m^{-2} ground), R_m is daily maintenance respiration (g C m^{-2} ground), *G* is daily gross growth expressed in units of carbon (g C m^{-2} ground), *S* is the variation of reserves (g C m^{-2} ground) and Y_g is the growth yield (g C g^{-1} C). As indicated in Section 2.1, these variables do not contain units of time because they are calculated in a daily discrete model where time is implicit. The growth yield varies during the year and can be calculated as:

$$Y_G = \frac{1}{\sum_{k=1}^{6} \frac{PC_k}{PV_k CC_k}} \quad (17)$$

Where *PC*, *PV* and *CC* are the partitioning coefficients (g C g^{-1} C), production values (g DM g^{-1} C) and carbon concentration (g C g^{-1} DM) of each organ *k* (see section 2.1.3 on Respiration), respectively. ρ is the ratio between total respiration and photosynthesis and α is the ratio between the daily variation of reserves and photosynthesis. When reserves are remobilized and used for growth, ρ can be higher than 1 and α will be negative, as a result of solving the system of equations 12-16. The equations presented in the above constrain the maximum and minimum values of ρ within the range:

$$\left(1-\alpha\right)\left(1-Y_g\right) < \rho < 1-\alpha \quad (18)$$

The value of ρ, α and Y_g were calculated from the simulations of the model using equations 12-16 and were compared with the theoretical ranges described by equation 18. This allowed to test if the values of ρ predicted by the model were physically possible and how far were they from the theoretical maximum and minimum. The dynamics of ρ during the year were analysed by segregating the effect of growth and maintenance respiration. In both case studies, the effect of plant age was analysed, as well as the effect of management system and climate in Case 2.

3. Results

3.1. Comparison with experiments

The growth of leaf area index was overestimated by the model during spring of each year (figure 2, A) and underestimated during the rest of the year, especially during the years with fruit production (1999-2002). At the end of each year, both measured and simulated LAI were similar. At the end of the fourth year, the model predicted a LAI of 1.82 m^2 leaf m^{-2} ground for an experimental value of 1.62 m^2 leaf m^{-2} ground. The differences between model and reality were caused by an overestimation of the growth rate of leaf area index during spring and almost no leaf growth during the period of fruit production. In the measurements, the daily growth rate of leaf area index was smaller but leaves kept growing for a longer period of time. Also, the simulations presented a sharp decrease of leaf area due

to senescence that was not present in the measurements. Only at the end of the experiment there was a decrease of leaf area index (figure 2, A).

The overestimation of LAI during spring caused a higher absorption of PAR during the first part of each year but similar values during the second half (figure 2, B). This resulted in a higher total absorption of PAR in the simulations. The annual trend of absorbed PAR was the result of the annual variation of incoming solar radiation and the growth of leaf area index, with a maximum value on the fourth year of simulation of 5.04 MJ PAR m^{-2} ground versus a maximum measured value of 4.52 MJ PAR m^{-2} ground. The maximum absorbed PAR was reached sooner each year of the simulation due to the overestimation of leaf area growth in spring.

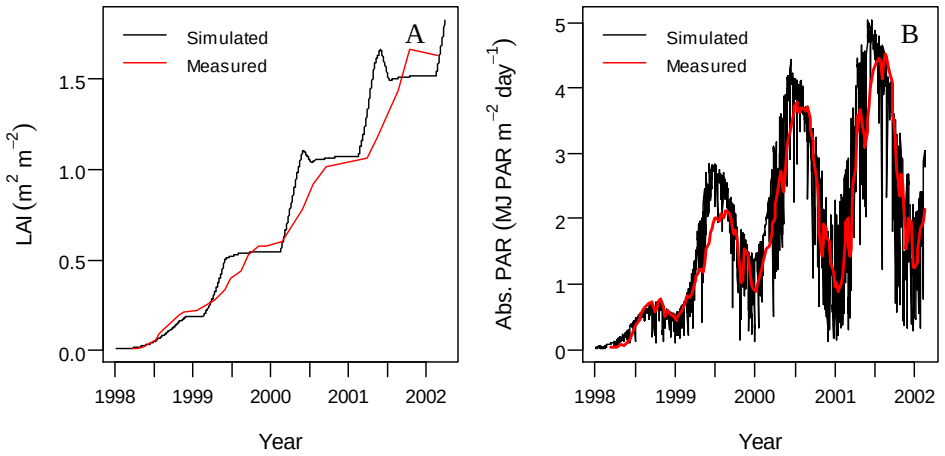

Figure 2: A. Simulated and measured leaf area index. B. Simulated and measured absorbed PAR. The measurements were performed on a high density olive orchard and the results are published in Villalobos et al. (2006).

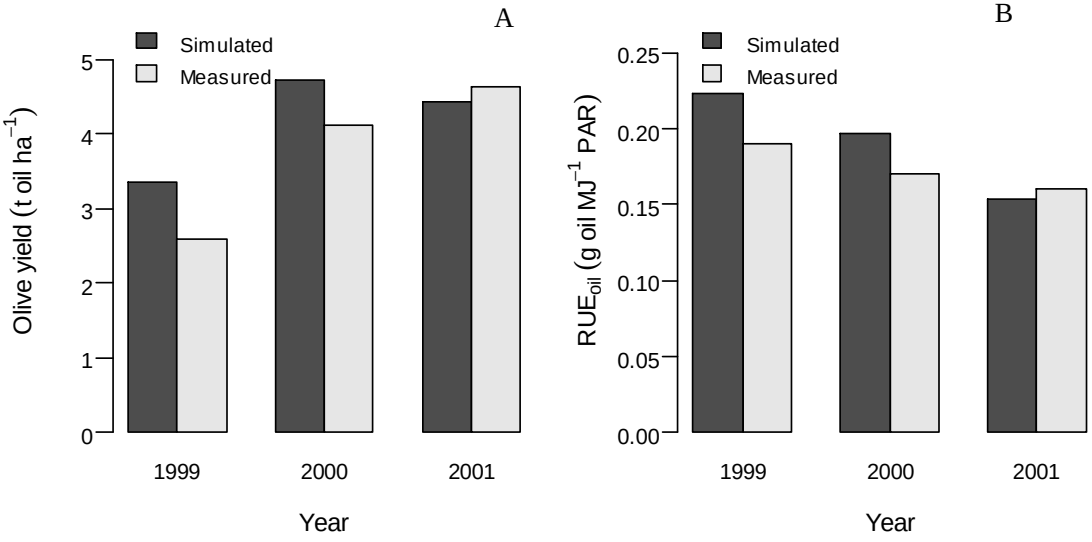

Figure 3: A. Simulated and measured fruit production per year. B. Simulated and measured radiation use efficiency for the production of oil. The measurements were performed on a high density olive orchard and the results are published in Villalobos et al. (2006).

The model overestimated the production of fruits during years 1999 and 2000, but obtained a very similar value on the year 2001 (figure 3, A). In the experiment, the production of fruits increased during three consecutive years from 2.6 t DM ha^{-1} up to 4.6 t DM ha^{-1}. The production on year 1999 was greatly overestimated by the model (3.4 t DM ha^{-1}) and slightly underestimated on the year 2001 (4.4 t DM ha^{-1}). The radiation use efficiency for the production of oil decreased with time in both the experiment and the simulation (figure 3, B): between 0.19 and 0.17 g oil MJ^{-1} PAR in the experiment and between 0.22 and 0.15 g DM MJ^{-1} PAR in the simulation.

In both the measurements and the simulations, the concentration of oil was quite constant and equal to 0.38 g oil g^{-1} DM fruit. The annual ratio between yield and gross biomass production aboveground decreased in the simulations from 0.54 in 1999 down to 0.41 in 2001, but in the experiment it was always above 0.54. The average annual gross biomass production during the four years of measurements was 5.6 t DM ha^{-1}, versus a value of 6.6 t DM ha^{-1} in the model. That is, the model overestimated biomass production by 19%.

Villalobos et al. (2006) did not report values of canopy photosynthesis but Testi et al. (2008) measured canopy photosynthesis with the eddy covariance technique in the same orchard. The measurements were discontinuous in time, covering the different seasons throughout the years of measurements. It showed a linear increase of canopy photosynthesis with leaf area index with a slope of 11.0 g CO_2 (m^2 leaf m^{-2} ground)$^{-1}$. Selecting from the simulation the days when Testi et al. (2008) performed their measurements, a slope of 10.8 g CO_2 (m^2 leaf m^{-2} ground)$^{-1}$ was obtained from the simulated values of canopy photosynthesis and leaf area index.

The model predicted a higher growth respiration during spring than in other seasons, as reserves were being used for vegetative growth (figure 4, A). The variability of growth respiration during the growing season was small. Maintenance respiration increased during the year following the trend of air temperature, reaching a maximum in August. The annual maximum increased with each consecutive year due to the accumulation of biomass (figure 4, A). Canopy photosynthesis increased during spring up to a maximum in the first half of June and presented a minimum at the end of December. The combination of the annual trends of the different fluxes described in the above, located the maximum net primary production (i.e. photosynthesis – respiration) in May, presenting small variations between August and January. Maximum photosynthesis, growth and maintenance respiration were 6.8, 1.4 and 5.3 g C m^{-2} ground day^{-1} and, since these maxima did not coincide in time, maximum net primary production was 3.5 g C m^{-2} ground day^{-1}.

The average ratio between respiration and photosynthesis (ρ) during the five years of simulation was 0.49. Note that fifth yera of the simulation has no correspondence with the experiment which only lasted for four years. The annual value of ρ increased from 0.32 in the first year up to 0.61 on the fifth year (figure 4, B). The values of ρ generated by the model were always within the theoretical ranges (figure 4, B), which varied greatly during the year due to the changes in the partitioning of assimilates and the remobilization of reserves. The annual trend of ρ was very similar during the simulated four years of fruit production: during the winter period of reserve accumulation, ρ was ca. 0.2, during the spring flush of growth, ρ increased up to 0.4 and during summer and autumn, it reached a maximum of 0.7-0.8, following, approximately, the seasonal trend of maintenance respiration.

Even though the production value of oil is much higher than for the other organs, the higher priority given to maintenance respiration in the distribution of assimilates meant that maintenance respiration dominated the dynamics of ρ during the period of fruit growth. Maintenance respiration represented only 30% of the total respiration at the beginning of spring of the first year but increased up to 95% during midsummer of the fifth year, with an average of 60%.

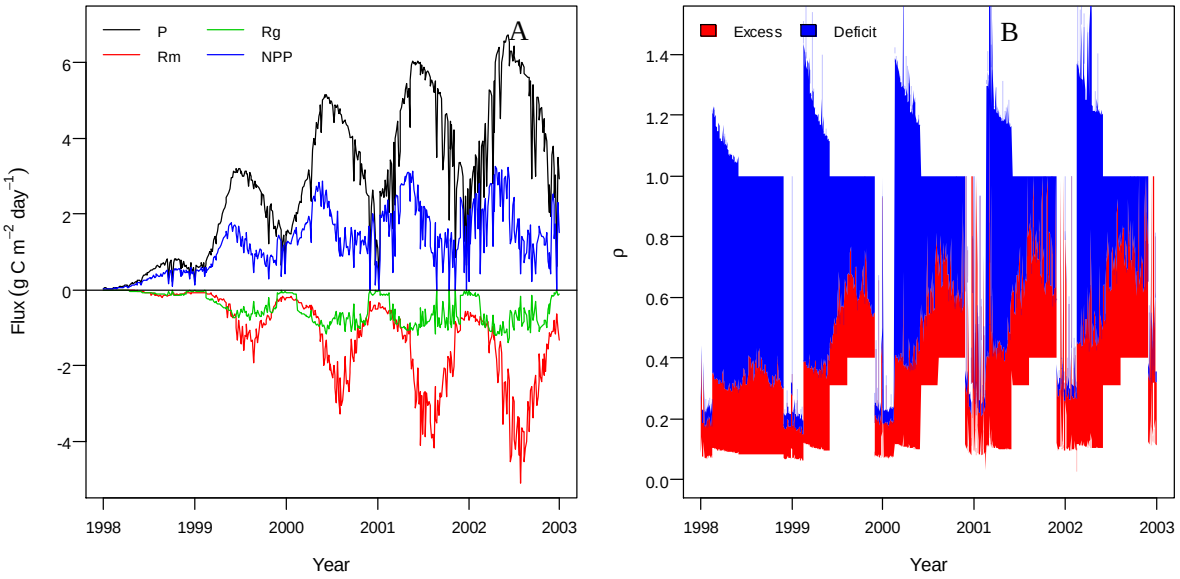

Figure 4: A. Time series of canopy photosynthesis (P), maintenance respiration (Rm), growth respiration (Rg) and net primary production (NPP), which is the difference between photosynthesis and both respirations. B. Ratio between total respiration and photosynthesis ($\rho = (R_g + R_m) / P$), and the area above the theoretical minimum (red) and below the theoretical maximum (blue). The limit between the red and blue areas represents the actual values of ρ.

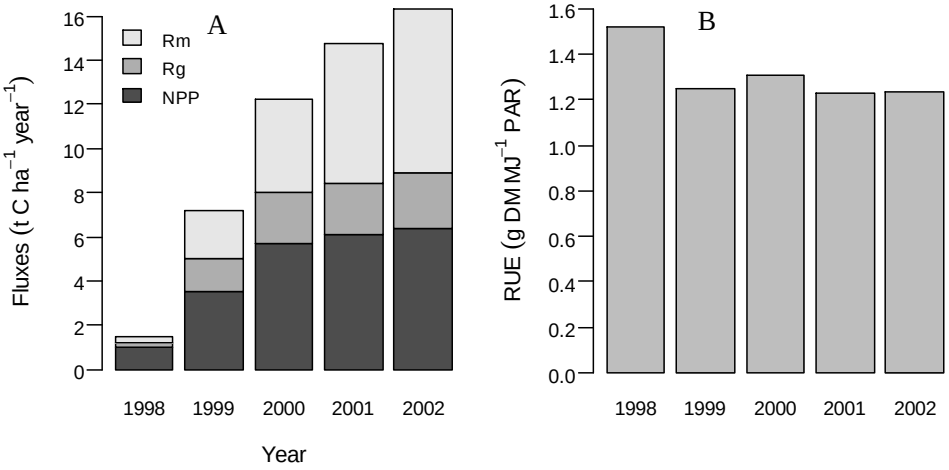

Figure 5: A. Components of the annual carbon balance of the olive trees disaggregated into net primary production (NPP), maintenance respiration (Rm) and growth respiration (Rg). B. Radiation use efficiency for total biomass production during the five years of the simulation.

Net primary production increased throughout the simulation but the differences in the last three years of the simulation were small, indicating a stabilization of annual growth (figure 5, A). Growth respiration increased proportionally to the annual net primary production, with a major increase between the first and second year when fruit production started. The annual values of maintenance respiration increased throughout the simulation without showing any stabilization (figure 5, A). On the first year of simulation, annual net primary production, growth respiration and maintenance respiration represented 0.68, 0.15 and 0.17 of annual photosynthesis, respectively. These fractions changed to 0.40, 0.15 and 0.45 on the fifth year. As the trees accumulated biomass, there was a clear transfer of assimilates from net primary production into maintenance respiration. Still, net primary production was 6.4 times higher on the fifth year compared to the first year, due to the increase of annual photosynthesis.

The annual radiation use efficiency for the production of total biomass decreased from a value of 1.52 g DM MJ^{-1} PAR during the first year to an average value of 1.25 g DM MJ^{-1} PAR during the following four years of fruit production, with small variations around this average (figure 5, B). These values correspond to 1.10 (first year) and 1.04 (average last four years) g DM MJ^{-1} PAR for the production of biomass aboveground. In the experiment, the RUE aboveground during the four years of measurements was 1.3, 0.9, 0.8 and 0.8 g DM MJ^{-1} PAR. Thus, the model underestimated the RUE aboveground of the first year and did not capture the decrease observed in the experiment in the following years, such that they were overestimated.

3.2. Effect of climate change on high and super-high density olive orchards

The dynamics of the leaf area index in the different simulations were determined primarily by the pruning of the trees (figure 6) and, although the pruning applied to high and super-high density orchards were based on different criteria (and none of them considered the leaf area index explicitly), the leaf area index after each pruning was very similar for both types of orchards and climate scenarios (2.2 and 2.4 m^2 leaf m^{-2} ground for high and super-high density orchards, respectively). Pruning started to be applied in the second year for all simulations except for the high density orchard under recent climate, where pruning started in the third year.

Once pruning started, leaf area index followed a recurrent annual trend with a maximum in late spring, a decrease due to senescence, a slight recovery during the phase of fruit production and a strong reduction due to pruning (figure 6). The annual gross growth of leaf area was lower under recent climatic conditions (average of 1.4 and 1.5 m^2 leaf m^{-2} ground for high and super-high density orchards, respectively) than under future climate conditions (average of 1.9 and 2.0 m^2 leaf m^{-2} ground for high and super-high density orchards, respectively). In the case of super-high density, the annual gross growth of leaf area decreased with the age of the plantation. The maximum leaf area index of the four simulations was achieved in the super-high density olive orchard under future climate, with a value of 5.1 m^2 leaf m^{-2} ground (figure 6, B), but only before pruning started.

The annual fraction of radiation absorbed by each orchard increased with the leaf area index stabilized at a maximum, once pruning started. At its maximum, the high density orchards absorbed 0.68 and 0.70 of the annual PAR during recent and future climate, whereas super-high density absorbed a slightly bigger fraction (0.71 and 0.73 for recent and future climate). The fraction of ground covered by the canopy varied each year following the variations of leaf area index, with a range of 0.45-0.55 and without significant differences among simulations.

The average oil concentration in high and super-high density olive orchards under recent climate conditions was 0.39 and 0.38 g oil g^{-1} DM, respectively, and increased by two points (i.e. 0.41 and 0.40 g oil g^{-1} DM) under future climate conditions. The overall variability of oil concentration in each simulation was small and was mainly explained by climate (standard deviations of 0.04 and 0.06 g oil g^{-1} DM under recent and future climate conditions, respectively).

In the high density olive orchard, maximum yield was obtained on the 6^{th} year under recent climate and on the 4^{th} year under future climate (figure 7, A). The maximum fruit production of the super-high density olive orchard occurred on the second year for both recent and future climate (figure 7, B). In the high density orchard, under recent climate, yield was rather stable after the maximum value had been reached, but in the rest of the simulations, yield decreased after reaching the maximum. In all the simulations, important variations were introduced by the weather each year. Future climate conditions increased the average fruit production from 8.0 up to 9.0 t DM ha^{-1} $year^{-1}$ in high density orchards and from 8.1 up to 8.3 t DM ha^{-1} $year^{-1}$ in super-high density orchards (figure 7). The variability was higher for super-high density orchards and future climate conditions and the standard deviation of yield increased from 1 up to 2 t DM ha^{-1} $year^{-1}$, when comparing high density and recent climate (minimum variability) with super-high density and future climate (maximum variability).

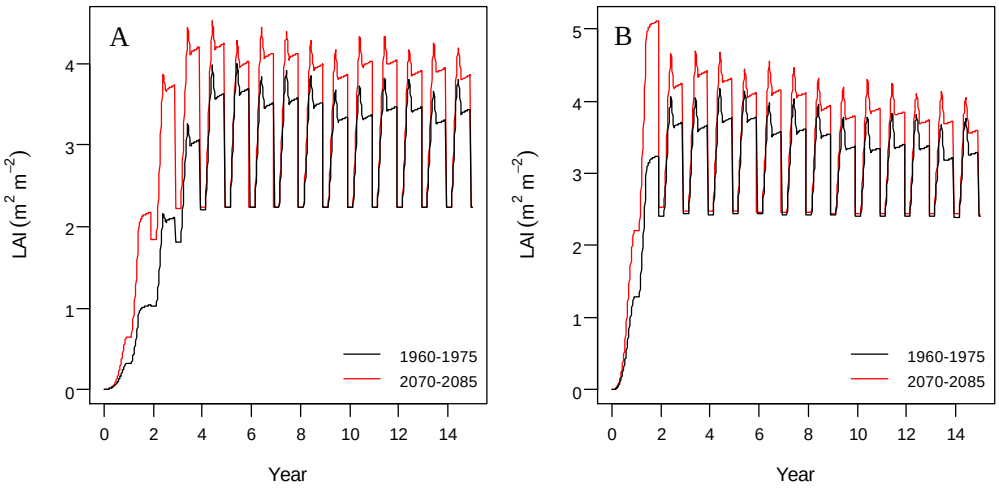

Figure 6: Leaf area index under past and future climate in high density olive orchards (A) and super-high density olive orchards (B).

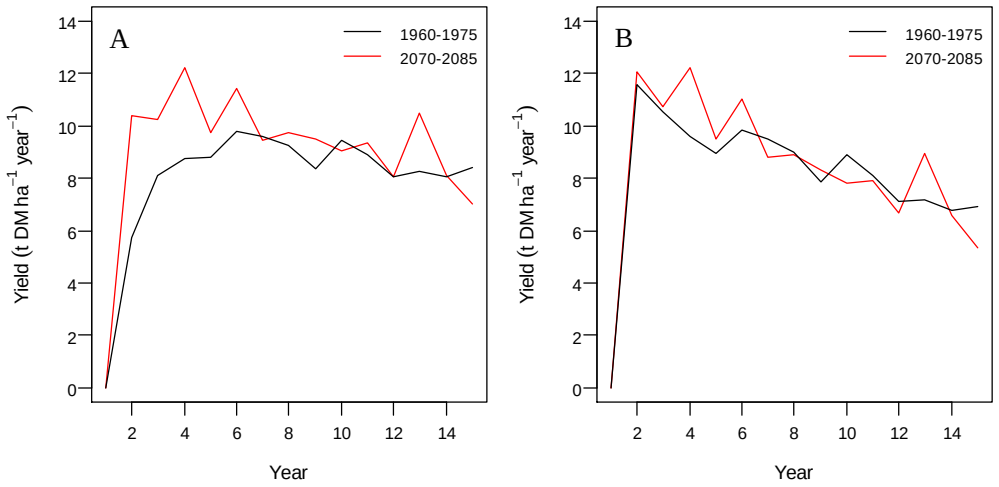

Figure 7: Fruit production under past and future climate in high density (A) and super-high density (B) olive orchards.

In the high density olive orchard (figure 8, A), maximum net primary production (13.5 t C ha^{-1} year^{-1}) was reached on year 8 under recent climate and on year 4 under future climate (16.5 t C ha^{-1} year^{-1}). Under future climate conditions, there was a slight decrease of the net primary production throughout the simulation, with an average rate of decrease of 0.3 t C ha^{-1} year^{-1}, whereas under recent climate, the net primary production stabilized at a value of 12.3 t C ha^{-1} year^{-1} for most of the simulation. Growth respiration followed the same patterns with an average of 4.8 and 5.3 t C ha^{-1} year^{-1} for recent and future climate, respectively. Maintenance respiration increased throughout the simulation for both recent and future climates, with maximum values of 14.1 and 21.8 t C ha^{-1} year^{-1}, respectively. On average, maintenance respiration was 65% higher under future climate conditions, whereas the average relative increase of annual photosynthesis was 45%.

In the super-high density olive orchard (figure 8, B), maximum net primary production (13.1 t C ha^{-1} year^{-1}) was reached on year 3 under recent climate and on year 2 under future climate (17.3 t C ha^{-1} year^{-1}). After the maximum had been reached, net primary production decreased continuously (figure 8, B) at an average rate of 0.3 and 0.4 t C ha^{-1} year^{-1} for recent and future climate, respectively. Growth respiration followed the same trend, with maximum values of 5.3 and 6.5 t C ha^{-1} year^{-1} for recent and future climate, respectively. Maintenance respiration increased throughout the simulation, with a higher rate during the first, unpruned years and an average increase of 47% under future

climate compared to recent climate, whereas the average relative increase of annual photosynthesis was 30%.

The annual ratio between total respiration and photosynthesis (ρ) increased with the age of the plantation in all the simulations (figure 9, A). The rate of increase was faster during the first years when no pruning was being applied. For all scenarios, annual ρ started at 0.33 and increased up to 0.60 and 0.66 for high density under recent and future climates, respectively, and 0.66 and 0.73 for super-high density under recent and future climates, respectively (figure 9, A). That is, the management system and climate had, each, a 10% effect on the annual value of ρ at the end of the simulation.

The first year of each simulation, maintenance respiration represented 0.53 of total respiration and this ratio increased to 0.70 and 0.79 for high density under recent climate and super-high density under future climate, respectively, with a similar effect of management and climate as for ρ. During the year, ρ followed the same seasonal pattern as in Case 1 (figure 4) and was always within the theoretical ranges. In most of the simulated years, ρ was always lower than 90% of the maximum theoretical value. But, in the last years of the super-high density orchard under future climate, the maximum theoretical value was reached during one third of the summer days. During those days, the model simulated no growth of the trees.

Annual radiation use efficiency for total biomass production increased when changing from recent to future climate conditions and from super-high density to high density orchards (figure 9, B). Whereas the differences due to climate were quite constant throughout the simulations, the effect of the type of orchard increased with time. In all the simulations, except for the high density orchard under recent climate, the radiation use efficiency decreased with the age of the plantations. In the high density olive orchard, the radiation use efficiency was very stable around a value of 1.15 g DM MJ^{-1} PAR, after the trees started to be pruned. Under future climate conditions, both types of orchards started with a RUE of 2.0 g DM MJ^{-1} PAR, whereas, under recent climate conditions, the initial RUE was 1.6 g DM MJ^{-1} PAR. At the end of the simulations, the differences due to climate were very small, with 1.15 and 0.95 g DM MJ^{-1} PAR for high density and super-high density orchards, respectively. The average relative increase of radiation use efficiency due to the effect of climate was 13 and 11% for high and super-high density orchards, respectively.

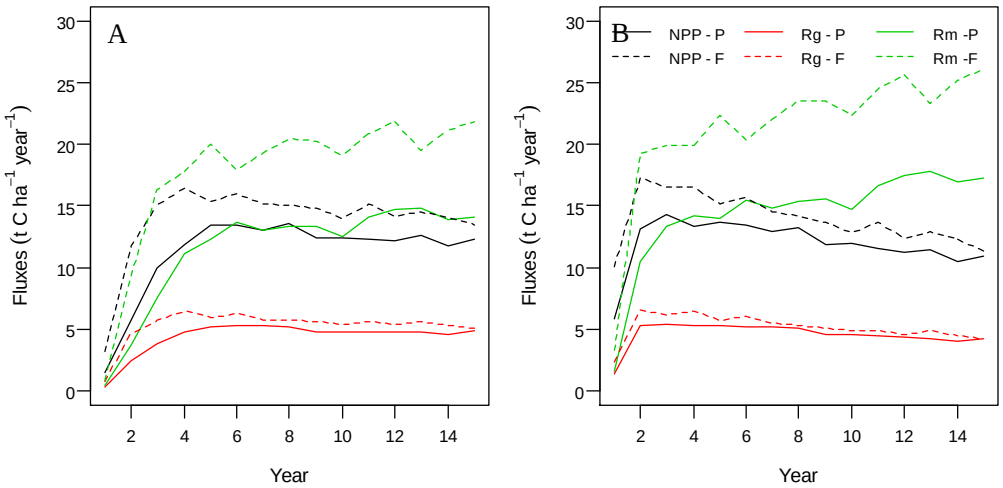

Figure 8: Components of the annual carbon balance of the olive trees disaggregated into net primary production (NPP), maintenance respiration (Rm) and growth respiration (Rg) in high density olive orchards (A) and super-high density olive orchards (B) for recent climate (P, solid lines) and future climate (F, dashed lines).

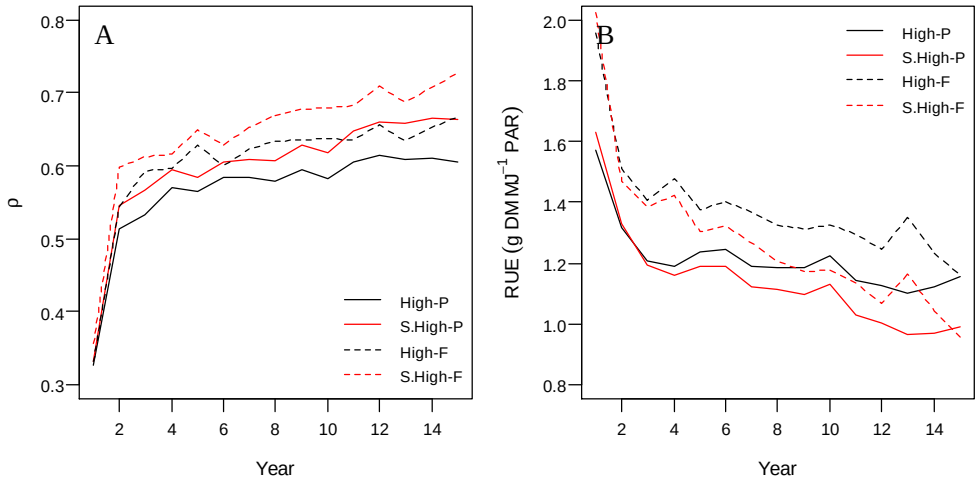

Figure 9: A. Ratio between respiration and photosynthesis (ρ) for recent (P, solid lines) and future (F, dashed lines) climate in high density and super-high density olive orchards. B. Radiation use efficiency of total biomass production for recent (P, solid lines) and future (F, dashed lines) climate in high density and super-high density olive orchards.

4. Discussion

4.1. Case 1

The model failed to predict accurately some of the observations reported by Villalobos et al. (2006):

1. Leaf area growth was over estimated during phenological phase 2 (spring) but underestimated in phases 3 and 4 (summer and autumn).

2. The production of fruits was overestimated, especially in 1999 and 2000, even though the harvest index was smaller than in the experiment.

3. The radiation use efficiency aboveground was overestimated in all years except, for the first one, and the decreasing trend observed in the experiment was not reproduced in the simulation.

However, it was successful in predicting the following:

1. The concentration of oil in fruits was the same as in the experiment.

2. The annual net increase of leaf area was very similar.

3. The amount of photosynthesis per unit of leaf area was very close to the value obtained by Testi et al. (2008).

In general, the discrepancies between the measurements and the predictions of the model are small. Integrating over the entire simulation, the model overestimated fruit production by 10%, leaf area production by 12% and aboveground biomass production by 19%. Given that the model has been calibrated with data from different experiments, it is a reasonable and satisfactory result. An important aspect of the experiment considered in Case 1 is the absence of pruning. This means that the part of the model concerned with pruning could not be tested in Case 1. Even if the performance of the model is considered satisfactory, it is important to investigate what may have caused the overestimation of the different outputs. The two most likely explanations for the discrepancies between model and reality are:

1. An underestimation of maintenance respiration: An underestimation of maintenance respiration will increase the radiation use efficiency, especially at the end of spring and during the summer, when maintenance respiration becomes the dominant component of total respiration, due to the higher temperatures. This would explain the overestimation of radiation use efficiency, leaf growth and fruit production. On the other hand, the average value of ρ was 0.49, which is within the

range of observed values for different C3 species (van Oijen et al., 2010). Part of the underestimation could be caused by the use of maintenance respiration coefficients for structural branches that are not corrected by the fraction of sapwood.

The literature contains a high variability of maintenance respiration coefficients, which indicates a high uncertainty about this flux. Some of the biochemical processes covered by the concept of maintenance respiration are not totally independent from growth (Cannell & Thornley, 2000). This could explain why the coefficients obtained by Perez-Priego et al. (*submitted*) were lower than the ones reported by Abdel-Razik (1989), who derived them from the biochemical composition of the different organs. There is a need for a better understanding of the maintenance respiration of olive trees.

2. An overestimation of the accumulation of winter reserves: An overestimation of the production of reserves during the winter would increase leaf growth during the phenological phase 2 (spring), which increases the amount of absorbed radiation and hence the production of fruits and total biomass. Also, since producing reserves is more efficient (in terms of carbon losses) than any other tissue, and since during the winter the maintenance respiration is at its minimum due to low temperatures, an overestimation of production of reserves will tend to increase the average radiation use efficiency at the annual scale. Since reserves are only used for vegetative growth, this would explain why fruit production was overestimated but the harvest index was underestimated.

An overestimation of the production of reserves in the model could be caused by the assumption of no root growth during the winter, and the assumption that photosynthesis is independent of the strength of assimilate demand, since, in reality, a very low demand of assimilates can reduce photosynthesis (Kirschbaum, 2011). There is a need to measure the carbon balance of olive trees during the winter, as well as the effect of sink strength on photosynthesis.

The experiment showed a continuous decrease of radiation use efficiency with time, whereas the model predicted very small interannual variations. The simulated daily radiation use efficiency varied in a wide range, with a maximum of 6.64 g DM MJ^{-1} PAR in spring (enhanced by remobilization of reserves) and a minimum during summer and winter due to high maintenance respiration and lack of growth, respectively. Mariscal et al. (2000b) calculated radiation use efficiency on a monthly basis and observed a similar annual pattern. Thus, although radiation use efficiency may be fairly constant on an annual scale it varies strongly on a seasonal level. The average radiation use efficiency for total biomass production during the years of fruit production (1.25 g DM MJ^{-1} PAR) was much smaller than the typical values reported for C3 crops (e.g. wheat with 2.6 g DM MJ^{-1} PAR, in Sinclair & Muchow, 1999). Crops with energy-rich seeds, such as soybean and peanut, have values of 2.0 g DM MJ^{-1} PAR or higher (Sinclair & Muchow, 1999), which indicates that the high production value of olives could not explain the discrepancy. For apple trees, Monteith (1977) obtained 2.8 g DM MJ^{-1} PAR, which indicates that the perennial nature of the olive tree is not a likely reason either. Runyon et al. (1994) calculated an average RUE of 1.3 g DM MJ^{-1} PAR under non-limiting conditions (i.e. without drought, frosts or extreme VPD) for different natural forests in Oregon, USA. Cannell et al. (1987) obtained a value of 1.6 g DM MJ^{-1} PAR for irrigated willow plantations. Thus, when compared with natural vegetation under potential conditions for growth, the values of radiation use efficiency calculated from the simulations seem reasonable. Hence, the low radiation use efficiency of olive trees could be caused by the lack of important genetic improvement in olive trees compared to other temperate fruit species (Fabbri et al., 2009).

4.2. Case 2

First, the effect of the management system (high density vs. super-high density orchards) will be discussed, using the simulations under recent climate. Then, the effect of climate will be analysed, comparing both climate scenarios and management systems.

4.2.1. Effect of management

The higher planting density in the super-high density olive orchard resulted in a higher fruit production and net primary production during the first years of the simulation, with a very similar radiation use efficiency to the high density orchard. The pruning of both types of orchards was such that, after the fourth year of plantation, the amount of radiation absorbed by the canopy as well as the production of assimilates via photosynthesis was similar for both types of orchards. However, since the mechanized pruning in the super-high density olive orchards did not remove any of the structural biomass, the increase of maintenance respiration, generated a decrease of net primary production, fruit production and radiation use efficiency. This was expressed by a divergence in the values of radiation use efficiency, which was the same for both orchards in the first year (1.6 g DM MJ^{-1}PAR) but differed at the end of the simulation (1.15 and 0.95 g DM MJ^{-1} PAR for high and super-high density orchards, respectively).

The average yield of the high density olive orchard was 8.00 t DM ha^{-1} $year^{-1}$, whereas for the super-high density orchard it was only 1.2% higher. Such a small increase was caused by a continuous decrease of yield after the early maximum had been reached. The average olive oil production was 3.2 t oil ha^{-1} $year^{-1}$, which is slightly higher than the maximum value of 3.0 t oil ha^{-1} $year^{-1}$ observed by Villalobos et al. (2006) for a wide range of orchards. It also agrees well with the maximum of 3.3 t oil ha^{-1} $year^{-1}$ measured by Pastor et al. (2007) in an experimental high density orchard cv. 'Arbequina' in Cordoba, Spain. For the same climate, Villalobos et al. (1994) reported potential oil yields of sunflower of 2.25 t oil ha^{-1}.

Assuming an energy content of 39.3 kJ g^{-1} oil (Merryl & Watt, 1973), the simulated average oil production is equivalent to 126 GJ ha^{-1} $year^{-1}$. Assuming a potential yield of 10 t DM ha^{-1} $year^{-1}$ for wheat and an energy content of 17.5 kJ g^{-1} DM (Merryl & Watt, 1973) in the grain, the potential yield of wheat is equivalent to 175 GJ ha^{-1} $year^{-1}$. Thus, once corrected for the energy content, the simulated olive oil yield is 72% of the potential wheat yield.

The total biomass produced during the simulations under recent climate scenario was 28% higher for the super-high density orchard, that is, the increase in total biomass was higher than for fruit biomass, which means that the harvest index had been reduced. Such reduction is explained by the increase of maintenance respiration, as this flux becomes more important during the summer due to the higher temperatures. That is, since maintenance respiration represents a bigger fraction of total respiration during the summer, its increase has a bigger effect on fruit production than on total growth.

However, Pastor et al. (2007) reported a strong decrease of yield in a super-high density orchard (from 19.5 down to 5.2 t DM ha^{-1} $year^{-1}$) after pruning started. Such decrease was explained by a strong decrease in the number of fruits that was not compensated by fruit weight. A similar strong decrease of yield was reported by De la Rosa et al. (2007) in a super-high density orchard cv. 'Arbequina' in Cordoba, Spain. This phenomenon is not captured by the model as it does not consider the number of fruits in the distribution of assimilates. In its current state, the model will overestimate fruit production of super-high density orchards if this collapse in yield occurs.

The ratio between total respiration and photosynthesis increased from a minimum at the beginning of the simulation of 0.33 (both types of orchards) up to 0.60 and 0.66 for the high and super-high density orchard, respectively. DeLucia et al. (2007) reported that, in forests, ρ increases with the age of the trees, observing a total range of variation of 0.17-0.77. Gifford (2003) reported a range of 0.35-0.60 for different forests and individual plants under controlled conditions. Also, the simulated ratio was always within the theoretical limits (van Oijen et al., 2010). A possible explanation for the strong increase in ρ during the simulation could be an overestimation of the maintenance respiration of the woody tissue as xylem tissue has a lower metabolic activity than the cortex. This makes sense as the model assumes that all the wood has the same respiration coefficient, whereas, in reality, most of the respiration is associated to the sapwood, which is a fraction of total wood biomass that decreases with tree age (Ryan, 1994). On the other hand, the experiment from which the coefficient was obtained (Perez-Priego et al., *submitted*) was performed on trees belonging to a 9 years old high density olive orchard, so that the sapwood biomass should not be too different in the simulations and the experiment.

4.2.2. Effect of climate

Under future climate conditions, both rates of photosynthesis and maintenance respiration increased. The higher rate of photosynthesis was caused by the fertilization effect of a higher atmospheric CO_2 concentration. The increase of air temperature and a higher biomass production were responsible for the increase of maintenance respiration. In relative terms, the increment of maintenance respiration was greater, as the ratio between respiration and photosynthesis increased. However, in absolute terms, photosynthesis was favoured more and the result was an increase of net primary production.

The average increase of photosynthesis for high and super-high density orchards was 45 and 30% respectively. Kirschbaum et al. (2011) reported a typical increase of photosynthesis of 30% under high CO_2 concentrations. The model could be overestimating photosynthesis under future climate conditions as acclimation of photosynthesis, that is, a reduction of photosynthesis due to low demand of assimilates (Kirschbaum et al., 2011), is not being taken into account. In any case, the simulations still show the importance of maintenance respiration in determining the productivity of the orchards and the interaction between pruning and climate.

The amount of absorbed radiation increased only slightly (2%) under future climate conditions, due to the control by pruning, whereas the net primary production was enhanced substantially (32 and 18% for high and super-high density orchards, respectively). This meant an average increase of 12% in the radiation use efficiency. The higher accumulation of biomass under future climate caused an increase in maintenance respiration. This caused a higher rate of decrease of radiation use efficiency compared to the simulations under recent climate. Thus, the radiation use efficiency was 25% higher in the first year, but fell to the same value on the last year of the simulation. This also means that the differences in biomass production between the super-high density and high density orchards were reduced to 13% with respect to the recent climate conditions where super-high density orchards produce 28% more biomass.

This increase was added to the effect of management (i.e. higher maintenance respiration for super-high density orchards) such that the effect was stronger in the case of the super-high density. This meant that, on the last year of the super-high density orchard, respiration consumed 72% of the annual assimilates generated by photosynthesis. Note that this is at the upper limit of the range observed by DeLucia et al. (2007). Because of this, under future climate conditions, oil production of the super-high density orchards was 28% less than to the high density orchard, even though photosynthesis was 3% larger.

At the end of the simulation, the carbon stored aboveground under the recent climate scenario was 12.2 and 59.9 t C ha^{-1} for the high and super-high density orchards, respectively. Under the future climate scenario, the final carbon storage aboveground was 10.7 and 71.9 t C ha^{-1} for the high and super-high density orchards, respectively. The type of pruning used in super-high density olive orchards results in a large accumulation of structural biomass, which increases under conditions of climate. However, in the case of the high density olive orchards, the maintenance of a certain leaf:wood ratio with a more selective pruning results in a lower value that decreases slightly under conditions of climate change.

5. Recommendations for further research

The construction and calibration of the model, as well as the analysis of the simulation have highlighted the following five aspects as the most important knowledge gap in our understanding of the carbon balance of olive trees.

1. Quantitative studies at the tree level of the dynamics of shoots, buds and fruits in consecutive years are needed to characterize alternate bearing. Without a quantification of the phenomenon it cannot be incorporated into the model. Even though the mechanisms underlying the

regulation and onset of alternate bearing may be unknown, a descriptive, quantitative approach will already increase the accuracy of the simulations.

2. Research is needed to understand the relative variations of photosynthesis and maintenance respiration, especially during winter and spring. It is important to quantify within which boundaries the ratio between respiration and photosynthesis varies and how it changes with the timescale.

3. Studies on the factors controlling maintenance respiration, such as nitrogen concentration or the fraction of active tissue in the total structural biomass, are needed to understand the discrepancies in the values reported in the literature.

4. A quantitative characterization of pruning is needed. Especially in terms of how much biomass of the different types of organs is removed and how this affects the leaf area density and crown dimensions.

6. Summary

1. On average, fruit production, leaf area index and biomass production aboveground were overestimated by the model (by 10%, 12% and 19%, respectively).

2. Radiation use efficiency increased under future climate conditions due to the stronger effect of CO_2 on photosynthesis than that of temperature on maintenance respiration.

3. Radiation use efficiency decreased in super-high density olive orchards as the pruning method did not affect the structural branches and the accumulation of this type of biomass increased the maintenance respiration.

4. The ratio between total respiration and photosynthesis was always within the theoretical boundaries and it increased with tree age, future climate and with super-high density management, for a total range of values of 0.32-0.72. The increase was caused by a stabilization of photosynthetic rates and an increase in the maintenance respiration.

References

Abdel-Razik, M., 1989. A model of the productivity of olive trees under optional water and nutrient supply in desert conditions. Ecological Modelling, 45(3): 179-204.

Ayerza, R. and Steven Sibbett, G., 2001. Thermal adaptability of olive (Olea europaea L.) to the Arid Chaco of Argentina. Agriculture, Ecosystems & Environment, 84(3): 277-285.

Bongi, G., Mencuccini, M. and Fontanazza, G., 1987. Photosynthesis of olive leaves - effect of light-flux density, leaf age, temperature, peltates, and H_2O vapour-pressure deficit on gas exchange. Journal of the American Society for Horticultural Science, 112(1): 143-148.

Bustan, A., Avni, A., Lavee, S., Zipori, I., Yeselson, Y., Schaffer, A.A., Riov, J. and Dag, A., 2011. Role of carbohydrate reserves in yield production of intensively cultivated oil olive (Olea europaea L.) trees. Tree Physiology, 31(5): 519-530.

Campbell, G.S., 1986. Extinction coefficients for radiation in plant canopies calculated using an ellipsoidal inclination angle distribution. Agricultural and Forest Meteorology, 36(4): 317-321.

Cannell, M.G.R. and Dewar, R.C., 1994. Carbon allocation in trees - a review of concepts for modelling. Advances in Ecological Research, 25: 59-104.

Cannell, M.G.R. and Thornley, J.H.M., 2000. Modelling the components of plant respiration: Some guiding principles. Annals of Botany, 85(1): 45-54.

Cannell, M.G.R., Milne, R., Sheppard, L.J. and Unsworth, M.H., 1987. Radiation Interception and Productivity of Willow. Journal of Applied Ecology, 24 (1): 261-278.

Castro-Diez, P. and Monserrat-Marti, G., 1998. Phenological pattern of fifteen Mediterranean phanaerophytes from Quercus ilex communities of NE-Spain. Plant Ecology, 139(1): 103-112.

Connor, D.J. and Fereres, E., 2005. The Physiology of Adaptation and Yield Expression in Olive, Horticultural Reviews. John Wiley & Sons, Inc., pp. 155-229.

De la Rosa, R., Leon, L., Guerrero, N., Rallo, L. and Barranco, D., 2007. Preliminary results of an olive cultivar trial at high density. Australian Journal of Agricultural Research, 58(5): 392-395.

De Melo-Abreu, J.P., Barranco, D., Cordeiro, A.M., Tous, J., Rogado, B.M. and Villalobos, F.J., 2004. Modelling olive flowering date using chilling for dormancy release and thermal time. Agricultural and Forest Meteorology, 125(1-2): 117-127.

deLucia, E.H., Drake, J.E., Thomas, R.B., Gonzalez-Melers, M., 2007. Forest carbon use efficiency: is respiration a constant fraction of gross primary production? Global Change Biology (13): 1157-1167.

Diaz-Espejo, A., Hafidi, B., Fernandez, J.E., Palomo, M.J. and Sinoquet, H., 2002. Transpiration and photosynthesis of the olive tree: A model approach. In: C.M.G.P. Vitagliano (Editor), Proceedings of the Fourth International Symposium on Olive Growing, Vols 1 and 2. Acta Horticulturae, pp. 457-460.

Diaz-Espejo, A., Walcroft, A.S., Fernandez, J.E., Hafidi, B., Palomo, M.J. and Giron, I.F., 2006. Modelling photosynthesis in olive leaves under drought conditions. Tree Physiology, 26(11): 1445-1456.

Eissenstat, D.M. and Yanai, R.D., 1997. The ecology of root lifespan. Advances in Ecological Research, Vol 27, 27: 1-60.

Ephrat, J.E., Goudriaan, J. and Marani, A., 1996. Modelling diurnal patterns of air temperature, radiation, wind speed and relative humidity by equations from daily characteristics. Agricultural Systems, 51(4): 377-393.

FAO Statistics Division, 2012. FAOSTAT, http://faostat.fao.org

Farquhar, G.D., Caemmerer, S. and Berry, J.A., 1980. A biochemical model of photosynthetic CO2 assimilation in leaves of C3 species. Planta, 149(1): 78-90-90.

Frabri, A., Lambardi, M. and Ozden-Tokatli, Y., 2009. Olive Breeding. In: S.M. Jain, P.M. Priyadarshan (eds.), *Breeding Plantation Tree Crops: Tropical Species*. Springer Science+Business Media, pp. 423-465.

Gifford, R.M., 1995. Whole plant respiration and photosynthesis of wheat under increased CO_2 concentration and temperature: long-term vs. short-term distinctions for modelling. Global Change Biology (1): 385-396.

Gifford, R.M., 2003. Plant respiration in productivity models: conceptualisation, representation and issues for global terrestrial carbon-cycle research. Functional Plant Biology, 30: 171-186.

Gomez-del-Campo, M., Centeno, A. and Connor, D.J., 2009. Yield determination in olive hedgerow orchards. I. Yield and profiles of yield components in north-south and east-west oriented hedgerows. Crop & Pasture Science, 60(5): 434-442.

Goudriaan, J. and van Laar, H. H., 1994. Modelling Potential Crop Growth Processes: Textbook with exercises. Kluwer Academic Publisher, Dordrecht, Netherlands, 251 pp.

Hermoso, J.F., Plana, J., Romero, A. and Tous, J., 2008. Performance of six olive oil cultivars in the south of Catalonia (Spain). In: M.T.L.S.F.L. Ozkaya (Editor), Proceedings of the Fifth International Symposium on Olive Growing, Vols 1 and 2. Acta Horticulturae, pp. 333-337.

IPCC, 2007. Climate Change 2007: Synthesis Report IPCC Fourth Assessment Report. Intergovernmental Panel on Climate Change, Geneva.

Jarvis, P.G. and McNaughton, K.G., 1986. Stomatal control of transpiration - scaling up from leaf to region. Advances in Ecological Research, 15: 1-49.

Kirschbaum, M.U.F., 2011. Does enhanced photosynthesis enhance growth? Lessons learned f rom CO_2 enrichment studies. Plant Physiology, 155: 117-124.

Koenker, R. and Hallock, K.F., 2001. Quantile Regression. Journal of Economic Perspectives, 15 (4): 143–156

Koenker, R. and Park, B.J., 1994. An Interior Point Algorithm for Nonlinear Quantile Regression, Journal of Econometrics, 71(1-2): 265-283.

Koenker, R., 2012. quantreg: Quantile Regression. R package. version 4.78. http://CRAN.R-project.org/package=quantreg

Lavee, S., 2007. Biennial bearing in olive (Olea europaea). Annales, Series Historia Naturalis, 17: 101-112.

Leuning, R., 1995. A critical-appraisal of a combined stomatal-photosynthesis model for C3 plants. Plant Cell and Environment, 18(4): 339-355.

Lloyd, J. and Taylor, J.A., 1994. On the temperature-dependence of soil respiration. Functional Ecology, 8(3): 315-323.

Loomis, R.S., Connor, D.J. and Cassman, K.G., 2011. Crop Ecology. Cambridge University Press, Cambridge.

Lopez, B., Sabate, S. and Gracia, C.A., 2001. Vertical distribution of fine root density, length density, area index and mean diameter in a Quercus ilex forest. Tree Physiology, 21(8): 555-560.

Luo, Y., Medlyn, B., Hui, D., Ellsworth, D., Reynolds, J. and Katul, G., 2001. Gross primary productivity in Duke forest: Modelling synthesis of CO_2 experiment and eddy-flux data. Ecological Applications, 11(1): 239-252.

Malik, N.S.A. and Bradford, J.M., 2005. Is Chilling a Prerequisite for Flowering and Fruiting in 'Arbequina' Olives? International Journal of Fruit Science, 5(3): 29-39.

Mariscal, M.J., Orgaz, F. and Villalobos, F.J., 2000a. Modelling and measurement of radiation interception by olive canopies. Agricultural and Forest Meteorology, 100(2-3): 183-197.

Mariscal, M.J., Orgaz, F. and Villalobos, F.J., 2000b. Radiation-use efficiency and dry matter partitioning of a young olive (Olea europaea) orchard. Tree Physiology, 20(1): 65-72.

Merino, J., 1987. The costs of growing and maintaining leaves of Mediterranean plants. In: J. Tenhunen, F.M. Catarino, O.L. Lange and W. Oechel (Editors), Plant response to stress. Functional analysis in Mediterranean ecosystems. NATO ISI Series. Springer Verlag, Berlin, pp. 553-564.

Merrill, A., L. and Watt, B., K., 1973. Energy values of foods: basis and derivation. Agricultural Handbook no. 74, Washington, DC, USA, pp. 105.

Milla, R., Castro-Diez, P., Maestro-Martinez, M. and Montserrat-Marti, G., 2005. Relationships between phenology and the remobilization of nitrogen, phosphorus and potassium in branches of eight Mediterranean evergreens. New Phytologist, 168(1): 167-178.

Monteith, J. L. and Moss, C. J., 1977. Climate and the efficiency of crop production in Britain [and discussion]. Philosophical Transactions of the Royal Society of London. Series B, Biological Sciences, 281: 277-294.

Morales, A., 2012. Measuring and modeling canopy photosynthesis of olive orchards. MSc Thesis Plant Production Systems, Wageningen University, 82 pp.

Moriana, A., Orgaz, F., Pastor, M. and Fereres, E., 2003. Yield responses of a mature olive orchard to water deficits. Journal of the American Society for Horticultural Science, 128(3): 425-431.

Moriana, A., Villalobos, F.J. and Fereres, E., 2002. Stomatal and photosynthetic responses of olive (Olea europaea L.) leaves to water deficits. Plant, Cell & Environment, 25(3): 395-405.

Norman, J.M. and Welles, J.M., 1983. Radiative Transfer in an Array of Canopies. Agronomy Journal, 75(3): 481-488.

Orgaz, F., Villalobos, F.J., Testi, L., Fereres, E., 2007. A model of daily mean canopy conductance for calculating transpiration of olive canopies. Functional Plant Biology 34, 178.

Orlandi, F., Lanari, D., Romano, B. and Fornaciari, M., 2006. New model to predict the timing of olive (Olea europaea) flowering: a case study in central Italy. New Zealand Journal of Crop and Horticultural Science, 34(1): 93-99.

Palese, A.M., Nuzzo, V., Dichio, B., Celano, G., Romano, M. and Xiloyannis, C., 2000. The influence of soil water content on root density in young olive trees. In: M.I.J.H.G. Ferreira (Editor), Proceedings of the Third International Symposium on Irrigation of Horticultural Crops, Vols 1 and 2. Acta Horticulturae, pp. 329-336.

Pastor, M., Garcia-Vila, M., Soriano, M.A., Vega, V. and Fereres, E., 2007. Productivity of olive orchards in response to tree density. Journal of Horticultural Science & Biotechnology, 82(4): 555-562.

Penning de Vries, F.W.T., Brunsting, A.H.M. and Van Laar, H.H., 1974. Products, requirements and efficiency of biosynthesis a quantitative approach. Journal of Theoretical Biology, 45(2): 339-377.

Perez-Priego, O., Testi, L., Orgaz, F. and Villalobos, F., Submitted. Plant respiration of an olive orchard. Functional Plant Biology.

Pope, V.D., Gallani, M.L., Rowntree, P.R. y Stratton, R.A., 2000. The impact of new physical parameterizations in the Hadley Centre climate model: HadAM3. Climate Dynamics, 16(2-3): 123-146

Priestley, C.A., 1977. Annual turnover of resources in young olive trees. Journal of Horticultural Science, 52(1): 105-112.

Proietti, P., 1998. Gas exchange in senescing leaves of Olea europaea L. Photosynthetica, 35(4): 579-587.

Proietti, P., Famiani, F. and Tombesi, A., 1999. Gas exchange in olive fruit. Photosynthetica, 36(3): 423-432.

Ruiz, E., Cara, C., Ballesteros, M., Manzanares, P., Ballesteros, I. and Castro, E., 2006. Ethanol production from pretreated olive tree wood and sunflower stalks by an SSF process. Applied Biochemistry and Biotechnology, 130(1-3): 631-643.

Runyon, J., Waring, R.H., Goward, S.N. and Welles, J.M., 1994. Environmental limits on net primary production and light-use efficiency across the Oregon transect. Ecological applications, 4(2): 226-237.

Ryan, M.G., 1990. Growth and maintenance respiration in stems of Pinus contorta and Picea engermannii. Canadian Journal of Forest Research, 20(1): 48-57.

Ryan, M., Linder, S., Vose, J. and Hubbard, R., 1994. Dark respiration of pines. Ecological Bulletins, 43, 50-63.

Scariano, L., Lo Bianco, R., Di Marco, L. and Policarpo, M., 2008. Dynamics of dry matter partitioning in young 'Nocellara del Belice' olive trees. In: M.T.L.S.F.L. Ozkaya (Editor), Proceedings of the Fifth International Symposium on Olive Growing, Vols 1 and 2. Acta Horticulturae, pp. 397-401.

Sinclair, T.R. and Muchow, R.C., 1999. Radiation use efficiency. Advances in Agronomy, 65: 215-265.

Sinoquet, H., Le Roux, X., Adam, B., Ameglio, T. and Daudet, F.A., 2001. RATP: a model for simulating the spatial distribution of radiation absorption, transpiration and photosynthesis within canopies: application to an isolated tree crown. Plant Cell and Environment, 24(4): 395-406.

Spitters, C.J.T., Toussaint, H.A.J.M. and Goudriaan, J., 1986. Separating the diffuse and direct component of global radiation and its implications for modeling canopy photosynthesis. Part I. Components of incoming radiation. Agricultural and Forest Meteorology, 38: 217-229.

Steven, M.D. and Unsworth, M.H., 1979. The diffuse solar irradiance of slopes under cloudless skies. Quart. J. Royal Met. Soc. 105: 593-602.

Testi, L., Orgaz, F. and Villalobos, F., 2008. Carbon exchange and water use efficiency of a growing, irrigated olive orchard. Environmental and Experimental Botany, 63(1-3): 168-177.

Tombesi, A., 1994. Olive fruit growth and metabolism. In: S. Lavee and I. Klein (Editors), II International Symposium on Olive Growing. International Society for Horticultural Science, Jerusalem, Israel.

Tous, J., Romero, A., Plana, J., 1998. Comportamiento agronómico y comercial de cinco variedades de olivo en Tarragona. Investigación Agraria: Producción y Protección Vegetal 13, 97-109.

van Nes, E., 2011. GRIND for MATLAB version 1.007. http://www.aew.wur.nl/UK/GRIND

van Oijen, M., Schapendonk, A., Hoglind, M., 2010. On the relative magnitudes of photosynthesis, respiration, growth and carbon storage in vegetation. Annals of Botany, 105: 793-797.

Vertregt, N. and Penning de Vries, F., 1987. A rapid method for determining the efficiency of biosynthesis of plant biomass. Journal of Theoretical Biology, 128(1): 109-119.

Ververis, C., Georghiou, K., Christodoulakis, N., Santas, P. and Santas, R., 2004. Fiber dimensions, lignin and cellulose content of various plant materials and their suitability for paper production. Industrial Crops and Products, 19(3): 245-254.

Villalobos, F.J., Sadras, V.O., Soriano, A., Fereres, E., 1994. Planting density effects on dry matter partitioning and productivity of sunflower hybrids. Field Crop Research 36, 1–11

Villalobos, F.J., Orgaz, F., Mateos, L., 1995. Non-destructive measurement of leaf area in olive (*Olea europaea* L.) trees using a gap inversion method. Agricultural and Forest Meteorology, 73: 29-42.

Villalobos, F.J., Testi, L., Hidalgo, J., Pastor, M. and Orgaz, F., 2006. Modelling potential growth and yield of olive (Olea europaea L.) canopies. European Journal of Agronomy, 24(4): 296-303.

Vossen, P. 2007. Olive oil: History, production, and characteristics of the world's classic oils. Hortscience, 42 (5): 1093-1100.

Zamora, R., Alaiz, M. and Hidalgo, F.J., 2001. Influence of cultivar and fruit ripening on olive (Olea europaea) fruit protein content, composition, and antioxidant activity. Journal of Agricultural and Food Chemistry, 49(9): 4267-4270.

Appendix I: Disaggregation of weather data

In this appendix, the algorithms used to disaggregate the daily weather data are described. In order to test the accuracy of the algorithms, the weather of year 2011 was recorded at a resolution of 10 minutes in a typical agricultural region of Cordoba, Spain (37° 44' N, 4° 36' W, altitude 170 m). The data was aggregated at the daily scale and the algorithms were used to reconstruct the original series from these daily values. Also, the parameters of the air temperature model were calibrated using this dataset. Note that these algorithms are not able to capture situations of heterogeneous cloudiness (i.e. where the fraction of the sky covered by clouds changes during the day), which can generate important outliers when comparing the calculated and measured values. However, they are able to capture, on average, the effect of different degrees of cloudiness on incoming radiation, temperature and vapour pressure deficit. The inputs to these algorithms are: Total daily solar radiation (MJ m^{-2} ground day^{-1}), daily maximum temperature (°C), daily minimum temperature (°C) and daily average vapour pressure (kPa). The outputs, which can be calculated at any time resolution, are total solar radiation and PAR (W m^{-2} ground) separated into direct and diffuse components, air temperature (°C) and vapour pressure deficit (kPa).

I.1. Solar radiation

This algorithm calculates incoming solar radiation and incoming photosynthetically active radiation (PAR), as well as its diffuse and direct components, as a function of the daily solar radiation. It is based on the algorithms proposed by Spitters et al. (1986) with some modifications in the notation introduced by Goudriaan & van Laar (1994). The modifications simplify the expressions and facilitate the comparison between the more comprehensive approach of Spitters et al. (1986) and the simpler, nested approach of Goudriaan & van Laar (1994). Thus, the equations presented in this section should not be compared directly with the equations in Spitters et al. (1986) and, specifically, the parameters *a* and *b* in equation A1 in this document are not related to the parameters *a* and *b* used in equation 5 in the article by Spitters et al. (1986).

Note that leap years are not considered and that the algorithm uses solar time[1]. Also, it is assumed that the field is horizontal and that there are no mountains or nearby infrastructures that could project shade on the field. The effect of slope is incorporated at a later stage in the model of radiation absorption by the canopy, using the approach of Steven & Unsworth (1979), but it will not be described in this document as it is not used in any of the simulations presented in this study.

This algorithm is assumed to have a wide generality and not to be dependent on local conditions, so the original parameterization is maintained. Its calculations were contrasted with the weather dataset to assess its accuracy. However, neither PAR nor the diffuse/direct fractions of radiation were measured by the weather station, so it was only possible to test the accuracy of the disaggregation of solar radiation corrected for the effect of cloudiness (Section I.1.1.1) but not corrected for the effects of Mie and Rayleigh scattering (Sections I.1.1.2 and I.1.1.3).

I.1.1. Solar radiation algorithm

In order to calculate the diurnal distribution of solar radiation, the angle between the sun and the horizon, known as the solar elevation angle (β, rad), is needed. The calculation of this angle only requires knowing the geographical latitude ($\lambda > 0$ for northern hemisphere, rad), the day of the year (*DOY*, 1 = 1st January, 365 = 31st December) and the time of the day (0 = midnight, 12 = solar noon). The solar elevation angle is calculated as:

[1] Solar time can be calculated by transforming local time into Greenwich Mean Time (GMT) and taking into account that every 5° of longitude to the West of the Greenwich Meridian subtracts 20 minutes.

$$\sin\beta = a + b\cos\left(2\pi\left(t-12\right)/24\right) \quad \text{(A1)}$$

Where $a = \sin\lambda \sin\delta$, $b = \cos\lambda \cos\delta$, δ is the declination angle (rad) and t is the time of the day. The declination angle changes during the year and it is caused by the orbiting movement of the Earth and the fact that the rotation axis is not perpendicular to the plane of the orbit. For each day of the year, the declination angle can be calculated as:

$$\sin\delta = -\sin\left(23.45\pi/180\right)\cos\left(2\pi\left(DOY+10\right)/365\right) \quad \text{(A2)}$$

Note that a, b, and δ are assumed constant within a given day. The time between sunset and sunrise (DL, h) is calculated as

$$DL = t_{ss} - t_{sr} = 12\left(1+\frac{2}{\pi}\text{asin}\left(a/b\right)\right) \quad \text{(A3)}$$

Where t_{ss} and t_{sr} are the times of sunset and sunrise (h) and asin represents the arc-sine trigonometric function. The amount of solar radiation incident on a horizontal plane, before entering the atmosphere, is known as the extra-terrestrial solar radiation[2] (S_0, W m^{-2}) and can be calculated as:

$$S_0 = S_k \sin\beta\left(1+0.033\cos\left[2\pi DOY/365\right]\right) \quad \text{(A4)}$$

Where S_k is the solar constant (1367 W m^{-2}) and the third factor in equation A4 describes the effect of the eccentricity of the Earth's orbit, which modifies the solar constant within the range 1320-1410 W m^{-2}. The extra-terrestrial solar radiation received on a given day ($S_{0,D}$, J m^{-2} ground day^{-1}) is obtained from the integration of equation A4, which analytical solution is known to be:

$$\begin{aligned} S_{0,D} &= \int_0^{24} S_0 \sin\beta dt = \\ &= S_k\left(1+0.033\cos\left[2\pi\left(DOY-1\right)/365\right]\right)3600\left(a\ DL+\frac{24}{\pi}b\sqrt{1-a^2/b^2}\right) \end{aligned} \quad \text{(A5)}$$

The ratio between the solar radiation on the surface of the Earth and the extra-terrestrial solar radiation is known as the atmospheric transmission coefficient. The daily atmospheric transmission (τ_D) is defined as:

$$\tau_D = \frac{S_{G,D}}{S_{0,D}} \quad \text{(A6)}$$

Where $S_{G,D}$ is the daily solar radiation (J m^{-2} ground day^{-1}). Assuming that the instantaneous transmission coefficient is constant during the day ($\tau = \tau_D$), the instantaneous solar radiation (S_G, W m^{-2} ground) can be calculated as:

$$S_G = S_0\frac{S_{G,D}}{S_{0,D}} = S_{G,D}\frac{\sin\beta}{\int_0^{24}\sin\beta dt} = S_{G,D}\frac{\sin\beta}{3600\left(a\ DL+\frac{24}{\pi}b\sqrt{1-a^2/b^2}\right)} \quad \text{(A7)}$$

However, empirical observations indicate that the instantaneous transmission coefficient is higher around solar noon than after sunrise or before sunset. This decrease of transmission towards the extremes of the day is caused by the increase in the optical thickness of the atmosphere (as solar beams have to travel a longer path through the atmosphere) and the occurrence of meteorological

[2] In order to facilitate the comparison with the existing literature, "extraterrestrial solar radiation" refers to the solar radiation above the atmosphere and "solar radiation" to the solar radiation after it has been filtered by the atmosphere, even though it is clear that all solar radiation is extraterrestrial due to its origin.

phenomena such as fog and low clouds (Spitters et al., 1986). A simple way to describe this variation is by introducing an additional dependency on the solar angle ($1 + c \sin\beta$) to equation A7:

$$S_G = S_{G,D} \frac{\sin\beta\left(1+c\sin\beta\right)}{\int_0^{24} \sin\beta\left(1+c\sin\beta\right) dt} = \\ = S_{G,D} \frac{\sin\beta\left(1+c\sin\beta\right)}{3600\left[DL\left[a+c\left(a^2+0.5b^2\right)\right]+\frac{24}{\pi} b\left(1+1.5c\,a\right)\sqrt{1-a^2/b^2}\right]} \quad \text{(A8)}$$

Using equations A1-A3 and A8, the daily total solar radiation can be disaggregated into the instantaneous solar radiation at any time of the day. Note that for $c = 0$, equation A8 is reduced to equation A7. To calculate how much radiation the canopy absorbs, one needs to separate the solar radiation into the its direct and diffuse components. The diffuse component is the fraction of solar radiation that is scattered by the particles in the atmosphere. The variations in the diffuse fraction of radiation is determined mainly by degree of cloudiness, which itself can be estimated by the atmospheric transmission coefficient. A first diffuse fraction can be calculated from the daily transmission coefficient (section I.1.1.1). However, depending on the size of the scattered relative to the wavelength of the radiation being scattered, two types of scattering can be distinguished:

1. Mie scattering is produced by particles of a size in the order of magnitude of the wavelength being scattered. In the atmosphere, dust and aerosols are responsible for Mie scattering of solar radiation. This scattering is not perfectly isotropic as the intensity of the scattered radiation is higher in the direction in which the radiation propagates.

2. Rayleigh scattering is produced by particles of a size much smaller than the wavelength being scattered. In the atmosphere, gas molecules are responsible for Rayleigh scattering of solar radiation. This scattering is perfectly isotropic but the intensity of the scattered radiation decreases with the wavelength.

The importance of these modifications to the spectral and spatial component of diffuse radiation depend on the solar elevation angle and the degree of cloudiness (Sections I.1.1.2 and I.1.1.3). The scattering of light by clouds is the result of multiple refractions and reflections of light as it interacts with water droplets and ice crystals. Thus, clouds generate an isotropic diffuse radiation without alterations of the solar spectrum.

I.1.1.1. Effect of cloudiness

The relationship between the daily diffuse fraction of radiation and atmospheric transmission coefficient is very similar for different locations of the Earth (Spitters et al., 1986) and can be described as:

$$\frac{S_{df,D}}{S_{G,D}} = \begin{cases} 1 & if\ \tau_D < 0.07 \\ 1-2.3\left(\tau_D-0.07\right)^2 & if\ 0.07 \le \tau_D < 0.35 \\ 1.33-1.46\tau_D & if\ 0.35 \le \tau_D < 0.75 \\ 0.23 & if\ 0.75 \le \tau_D \end{cases} \quad \text{(A9)}$$

where $S_{df,D}$ is the daily diffuse solar radiation (J m^{-2} day^{-1}). Whereas the instantaneous transmission coefficient changes during the day as described (implicitly) by equation A8, the ratio S_{df}/S_0, where S_{df} is the instantaneous diffuse solar radiation (W m^{-2}), is assumed to be constant during the day, that is, $S_{df,D}/S_{0,D} = S_{df}/S_0$. This simplification is based on the fact that the reflection and absorption of solar radiation by the clouds and other scatterers will tend to compensate the increase in the diffuse fraction. Thus, the diurnal variation of the diffuse fraction of solar radiation (S_{df}/S_G) is determined by τ

(i.e. $f_D = S_{df,D}/(\tau\, S_{0,D})$). Thus, the fraction of diffuse radiation is higher after sunrise and before sunset (low τ) and lower in the central hours of the day (high τ). If the day being simulated is characterized by intermittent cloudiness, the diurnal evolution of f_D may not follow this pattern.

I.1.1.2. Effect of Mie scattering

In order to take into account the effect of Mie scattering (i.e. higher diffuse radiation in the direction of the sun), the additional radiation corresponding to this effect is calculated, subtracted from the diffuse solar radiation and added to the direct solar radiation. This way, the model can still assume an isotropic distribution of diffuse radiation, which simplifies the calculations, but the effect of Mie scattering is considered. The new corrected daily diffuse radiation ($S'_{df,D}$, J m^{-2} day^{-1}) is calculated as:

$$S'_{df,D} = \frac{S_{df,D}}{1+\left(1-\left(\frac{S_{df,D}}{S_{G,D}}\right)^2\right)\cos^2\left(\frac{\pi}{2}-\overline{\beta}\right)\cos^3\left(\overline{\beta}\right)} \qquad \text{(A10)}$$

Where $\overline{\beta}$ is the average daily solar elevation angle. This correction is especially important in days with low cloudiness and intermediate solar elevation angles (figure A1). The maximum correction is a reduction of 15%, obtained on a day without clouds and a daily average solar elevation of 45°. The mean daytime solar elevation angle may be calculated by integrating numerically equation A1 between sunrise and sunset. As a reference, for a latitude of 37.5° North, the daytime average solar elevation varies from 18.6° up to 40.9° (figure A2).

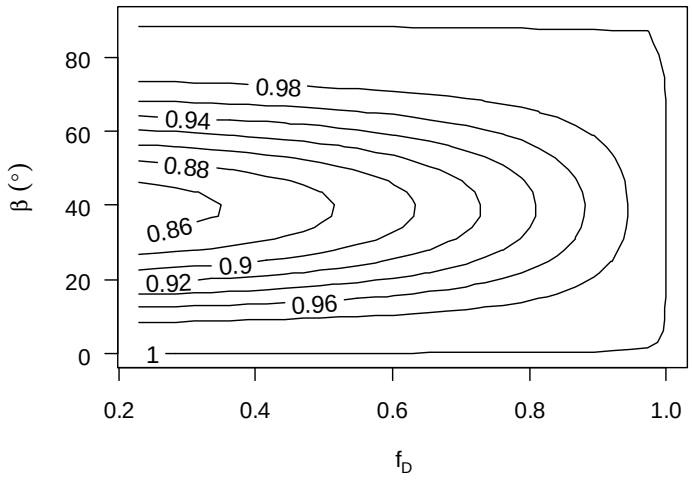

Figure A1: Contour plot representing the fraction of diffuse after the circumsolar correction relative to the diffuse fraction before the correction, versus the uncorrected diffuse fraction (f_D) and the daily average solar angle (β).

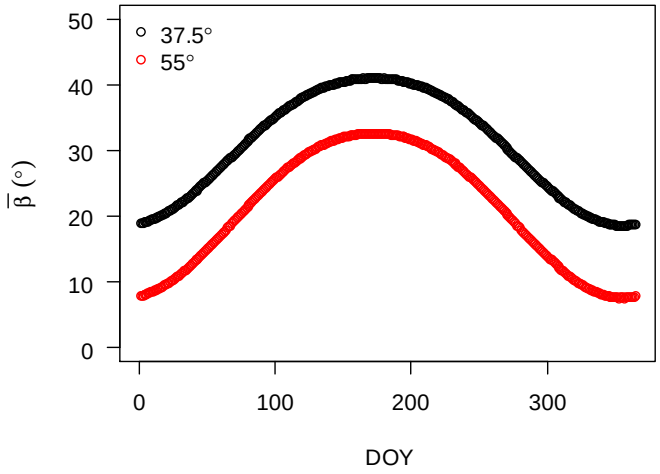

Figure A2: Daytime average solar elevation during the year for a latitude of 37.5 °N and 55 °N.

I.1.1.3. Effect Rayleigh scattering

The photosynthetically active radiation (PAR) is assumed to be 50% of the solar radiation (S_G), but the scattering due to the Rayleigh effect is higher for PAR than for solar radiation. Weighting by the effect of the different wavelengths on photosynthesis, Spitters et al. (1986) proposed to use the following expression:

$$\frac{PAR_{fd,D}}{PAR_{G,D}} = \left[1+0.3\left(1-\left(\frac{S_{fd,D}}{S_{G,D}}\right)^2\right)\right]\frac{S'_{fd,D}}{S_{G,D}} \qquad \text{(A11)}$$

Where the subscripts for PAR have the same meaning as for solar radiation. The correction due to Mie scattering reduces the diffuse fraction but the correction due to Rayleigh scattering increases it and the result is that the diffuse fraction of PAR is always higher than the uncorrected fraction calculated with equation A9. This increase is higher for clear-sky days and for low and high solar angles (figure A3).

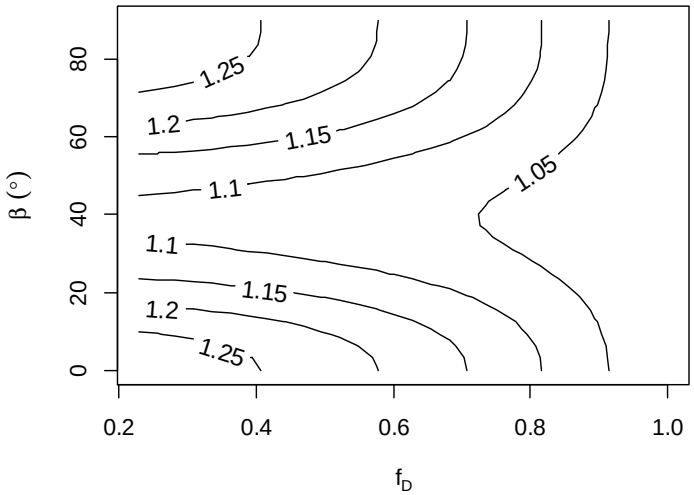

Figure A3: Contour plot indicating the fraction of diffuse PAR relative to the uncorrected fraction of diffuse solar radiation, for different values of the angle of solar elevation (β) and the uncorrected diffuse fraction of total solar radiation (f_D).

I.1.2. Test of the solar radiation algorithm

The predictions of S_G by the algorithms were compared with the measurements of S_G at intervals of 10 minutes. The comparison was made with the original value of c = 0.4 and with a value of c = 0, which corresponds to the simplified approach (equation A8). The mean absolute error decreased from 61 W m^{-2} ground for c = 0 to 55 W m^{-2} for c = 0.4 (figure A4), indicating a small improvement in the predictions. The change of accuracy was concentrated primarily on the highest radiation fluxes, which were underestimated for c = 0 and overestimated (but closer to the true value) for c = 0.4. This suggests that the optimal c for that dataset will be an intermediate value. The residuals were not homogeneous and the maximum deviations occurred in the range of 400-600 W m^{-2} ground. The deviations between the model and the data were higher during winter time (figure A4) although strong deviations still existed in specific days throughout the year.

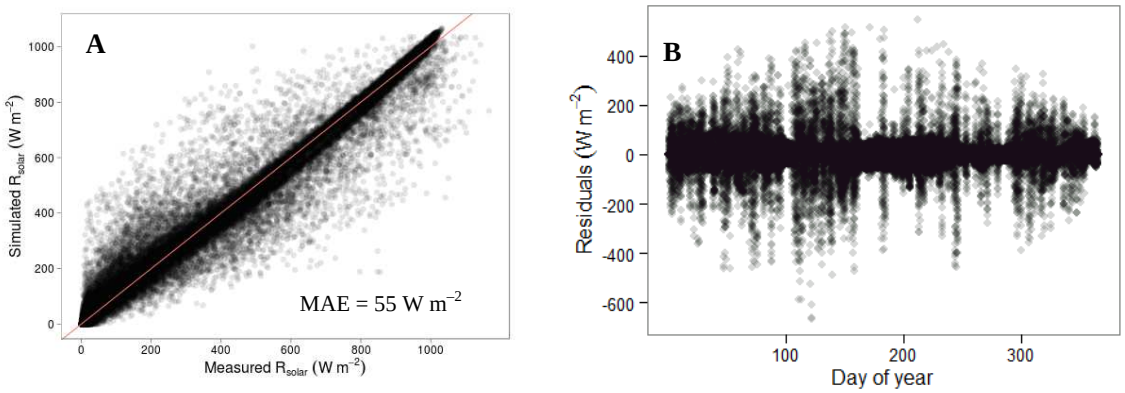

Figure A4: Comparison between simulated and measured solar radiation using the variation of atmospheric transmisivity during the day with a value of c = 0. 4 (A) and distribution of the residuals during the year (B). MAE is the mean absolute error.

I.2. Air temperature

This algorithm calculates the variation of air temperature during the day as a function of daily maximum and minimum temperature registered by a weather station. The spatial variations in temperature are not taken into account (i.e. the temperature generated by the algorithm refers to the location and height where the input data was measured). The modified sine-exponential model described in Ephrat et al. (1996) was used, which is a generalization of the sine-exponential model described by Goudriaan and van Laar (1994). The generalization includes the effect of buoyancy on turbulent mixing, which will affect the process of heating and cooling of the air during the day. Ephrat et al. (1996) showed how the generalization improved the disaggregation of air temperature in Israel and California, both having Mediterranean climates. Given that olive trees are cultivated predominantly in areas with Mediterranean climate, the model of Ephrat et al. (1996) is an interesting improvement. Since the parameters of the model are site-specific, it was calibrated, using the same weather dataset as for the solar radiation algorithm. The model uses different approaches to simulate the changes of air temperature during daytime (section I.2.1) and night-time (section I.2.2).

I.2.1. Daytime air temperature

The original sine-exponential model assumes that air temperature varies as a sine function of time where the minimum temperature occurs p_1 hours after sunrise and maximum temperature occurs p_2 hours after noon (assuming solar time). Thus, the relative variation of temperature during the day is described by the expression:

$$S = \sin\left(\pi \frac{t - p_1 - 12 + DL/2}{DL + 2p_2}\right) \quad \text{(A12)}$$

Where t is the time of the day (h) and DL is time between sunset and sunrise (h). The amplitude of the sine wave is determined by the maximum (T_{max}, °C) and minimum temperature, although the minimum temperature to be used depends on the part of the day being simulated. That is, before maximum temperature is reached, the minimum temperature of that day is used (T_{min}, °C) and after maximum temperature has been reached, the minimum temperature of the next day (T_{minA}, °C) is used:

$$T_{air} = \begin{cases} T_{min} + (T_{\max} - T_{min})S & if \;\; t_{sr} + p_1 < t < 12 + p_2 \\ T_{\min A} + (T_{\max} - T_{\min A})S & if \;\; 12 + p_2 < t < t_{ss} \end{cases} \quad \text{(A13)}$$

As the day advances, the turbulent intensity generated by buoyancy increases, which enhances the mixing of the different layers of air and the release of heat from the surface of the soil. This phenomenon is especially important whenever a strong vertical gradient of air temperature is formed. The effect of this enhanced mixing is accelerating the rate of heating during the first half of the day and decreasing the rate of cooling during the second half of the day (which "flattens" the diurnal temperature curve in the afternoon). Ephrat et al. (1996) proposed to incorporate this effect by multiplying equation A12 by a function of air temperature:

$$S_b = \frac{S}{1 + \frac{1}{T_K}(T_{air} - T_{min})} = \frac{S}{1 + I_k (T_{air} - T_{min})} \quad \text{(A14)}$$

Where S_b is the modified sine wave and T_k (°C) is the temperature increment at which the transport rate of heat doubles, due to buoyancy, when compared with the situation of no buoyancy. I_k (°C^{-1}) is simply the inverse of T_k. For a given T_k, the effect of buoyancy increases with $T_{air.}$ For a given T_{air}, the effect of buoyancy decreases with T_k. Note that $S_b = S$ for $T_k \rightarrow \infty$. Since equation A14 is a generalization of equation A12, it is interesting to use the second parameterization, with $I_k = 1/T_k$, as then we obtain the equivalence between both equations for an exact value of $I_k = 0$ as opposed to $T_k \rightarrow \infty$. This is especially useful when calibrating the model as, for situations of little or no effect of buoyancy, I_k will tend to 0 as opposed to ∞. In any case, T_{air} is an implicit function in equation A14, which means that the generalized form of equation A13 has to be rearranged. Ephrat et al. (1996) gave the solution to this problem which, when expressed in terms of I_k is:

$$T_{air} = T_{min} - \frac{1}{2I_k} + \frac{1}{2}\sqrt{\frac{1}{I_K^2} + 4(T_{max} - T_{min})\left(\frac{1}{I_k} + T_{max} - T_{min}\right)S} \quad \text{(A15)}$$

Unfortunately, this solution is still undetermined when using $I_k = 0$, but, at least, it behaves adequately as I_k approaches to 0 (figure A5). Therefore when $I_k = 0$, equation A13 is used and when $I_k > 0$, equation A15 is used. In order to ensure continuity (as I_k is a real number), a tolerance value of 10^{-15} can be used, although this is a technical problem that will depend on the programming language and computer being used. The values of p_1, p_2 and I_k will vary with the vegetation cover, soil water content and other biotic and abiotic factors affecting the temporal dynamics of air temperature. Thus, it is expected to vary for different locations, climates and even seasons (Ephrat et al. 1996).

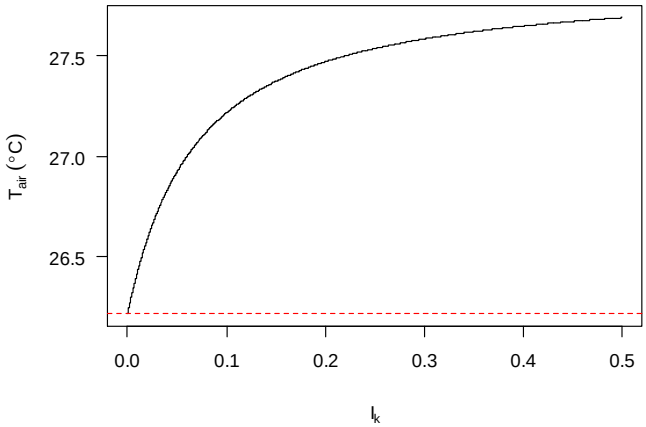

Figure A5: Air temperature as a function of the parameter I_k that determines the effect of turbulent mixing in the atmosphere due to buoyancy. The calculations were done for 1800 solar time for a daylength of 12 hours, maximum and minimum temperature of 20 and 30 °C, a time lag of 1.5 h between maximum temperature and solar radiation and a time lag of 0.2 h between minimum temperature and sunrise. The solid black line represents the calculations varying I_k and the dashed red line the value of I_k = 0.

I.2.2. Night-time air temperature

During the night, the changes of air temperature are determined by the radiative cooling of the surface: as the soil and plants release energy through thermal radiation, they cool down and, through convection, they air close to this surface also cools down. This process can be described by an exponential decrease of temperature determined by a time coefficient (*TC*, h). The time coefficient evaluates how fast the surface cools during the night. For technical reasons, one has to split this curve into two parts, before and after midnight, since the model of carbon balance simulates day by day. For these two parts, night-time air temperature can be described as

$$T_{air}(t) = \begin{cases} \dfrac{T_{\min A} - T_{ss}e^{-NL/TC} + \left(T_{ss} - T_{\min A}\right)e^{-(t-t_{ss})/TC}}{1-\mathrm{e}^{-NL/TC}} & if\ \ t_{ss} < t < 24 \\ \dfrac{T_{min} - T_{ssB}e^{-NL/TC} + \left(T_{ssB} - T_{min}\right)e^{-(24+t-t_{ssB})/TC}}{1-\mathrm{e}^{-NL/TC}} & if\ 0 < t < t_{sr} + p_1 \end{cases} \quad \text{(A16)}$$

Where T_{ss} and T_{ssB} are the air temperature (°C) at sunset calculated on the day of interest and on the day before, respectively, *NL* is the length of the night (i.e. n = 24 - *DL*) and t_{ssB} is the time of sunset of the day before. The value of *TC* depends on different local factors, including the type of vegetation cover and the soil water content of the soil.

I.2.3. Calibration

The parameters p_1, p_2, I_K and *TC* were estimated from the same weather dataset used in the previous section. Given that irregular cloudy conditions may generate strong outliers in the calibration, a robust method of non-linear regression was used. Specifically, a median regression, based on the interior point method (Koenker & Park, 1994) was used. Median regression belongs to the more general concept of quantile regression (Koenker & Hallock, 2001) which avoids making probabilistic assumptions about the nature of the residuals (i.e. it is a non-parametric regression method). Note that, mathematically, the result of a median regression coincides with the result of minimizing the sum of absolute deviations, assuming that the global optimum is found with this second approach. The calibration was implemented with the package 'quantreg' for the R programming language (Koenker, 2012).

The calibration resulted in a value of 0 for I_K (Table A1), indicating that the effect of buoyancy was not important. The calibration was also performed for each individual season of the year (results not shown) and always resulted in a negligible value for I_K. This contrasts with the values obtained by Ephrat et al. (1996) which range from 0.64 to 3.03 °C^{-1}, although the calibration was performed with individual days and only with daytime data. Since, in this study, all the parameters are calibrated at once with both night-time and daytime measurements, the compensation effects among the parameters of the model could be responsible for assigning an optimal null value to I_k.

The delay between solar noon and maximum temperature (table A1) was also bigger than the typical values in the range 1.5 – 2 h (Goudriaan and van Laar, 1994; Ephrat et al. 1996) but smaller than the value reported by Ephrat et al. (1996) for California (3.5 h). Ephrat et al. (1996) observed values of TC between 3 – 5 hours, which are smaller than the ones obtained in this study (table A1).

The mean absolute error was 1 °C and it was higher for intermediate temperatures (figure A6). The diurnal curves of air temperature, especially during clear-sky days, show a clear exponential decrease of temperature during the night and a sinusoidal variation during the day, as predicted by the model (figure A6).

Table A1: Optimal parameters for the model of air temperature using one year of weather measured at intervals of 10 min. I_k is the parameter related to the effect of buoyancy, p_1 and p_2 are the delays of minimum and maximum temperature with respect to sunrise and solar noon, respectively. *TC* is the time coefficient of the night-time exponential decline of temperature.

	I_K (°C $^{-1}$)	p_1 (h)	p_2 (h)	*TC* (h)
Optimal value	0.00	0.47	2.86	6.31

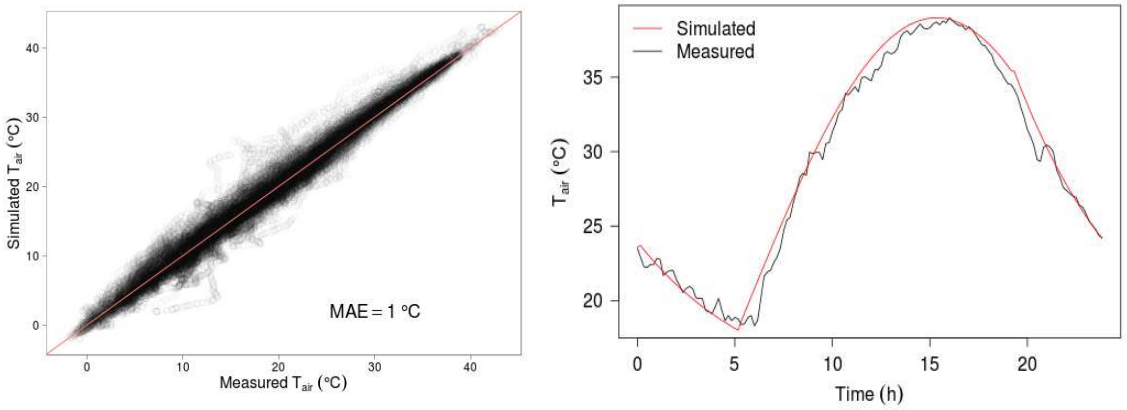

Figure A6: Comparison of measured and simulated values of air temperature (left) for the entire weather dataset. Comparison of diurnal trend of simulated and measured air temperature during DOY 180. MAE is the mean absolute error.

I.3. Vapour pressure deficit

It is assumed that vapour pressure is constant during the day, as diurnal fluctuations of this variable are generally small (Goudriaan and van Laar, 1994). The vapour pressure deficit (*VPD*, kPa) is calculated as:

$$VPD = e_{s,a} - e_a \qquad \text{(A17)}$$

Where $e_{s,a}$ is the vapour pressure of saturated air (kPa) and e_a is the actual vapour pressure (kPa). The vapour pressure deficit in air increases with air temperature, as hotter air is able to store more water vapour. In the range of 0-50 °C and when the main source of water vapour is liquid water, this increase can be computed as (Murray, 1967):

$$e_{s,a} = 0.611 \exp\left[\frac{17.3 T_{air}}{237.3 + T_{air}}\right] \quad \text{(A18)}$$

Where T_{air} is the temperature of the air (°C), generated by algorithm described on section I.2. The daily average e_a was used to calculate the vapour pressure deficit with the simulated $e_{s,a}$ using equation A17. The weather station does not measured directly the vapour pressure deficit, so that a "measured" $e_{s,a}$ was calculated from measured air temperature and equation A18 and, with the measured relative humidity ($RH = e_a/e_{s,a}$), the "measured" vapour pressure deficit was obtained. Both calculations agree well with each other, with a mean absolute error of 0.06 kPa, although the algorithm tend to overestimate vapour pressure deficit at high values (figure A7).

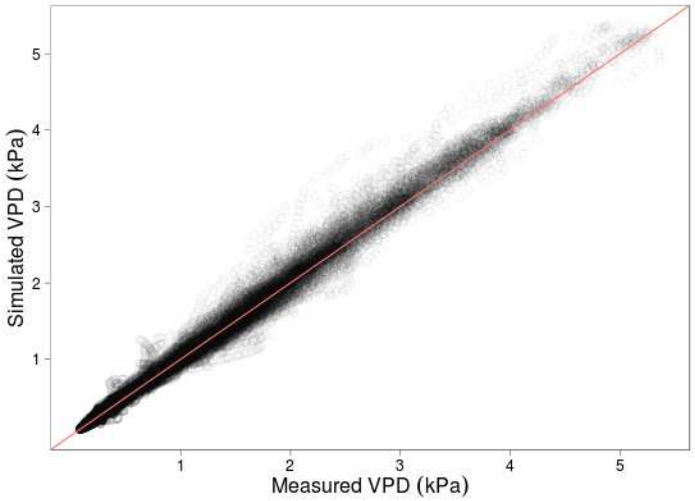

Figure A7: Simulated and measured vapour pressure deficit (VPD) for the entire weather dataset.